

**Remote Seismicity Activation in Japan:  
Triggering and Decay Characteristics**

February 2018

**ANCA OPRIS**

**Remote Seismicity Activation in Japan:  
Triggering and Decay Characteristics**

A Dissertation Submitted to  
the Graduate School of Life and Environmental Sciences,  
the University of Tsukuba  
in Partial Fulfilment of the Requirements  
for the Degree of Doctor in Philosophy in Science  
(Doctoral Program in Earth Evolution Sciences)

**ANCA OPRIS**

# Contents

<b>Abstract</b>	i
<b>List of Figures</b>	iv
<b>List of Tables</b>	vi
<b>Chapter 1 Introduction</b>	
1.1 Background: earthquake triggering mechanism	1
1.2 Review of decay characteristics of earthquakes	4
1.3 Research purpose and objectives	6
<b>Chapter 2 Triggering case of the 2011 M6.4 Shizuoka earthquake sequence</b>	
Abstract	8
2.1 Introduction	9
2.2 Method and data	12
2.3 Results and discussions	21
2.4 Conclusions	30
<b>Chapter 3 Remote triggering in Southwest Japan</b>	
3.1 Introduction	31
3.2 Method and data	33

<b>3.3</b>	Dynamic triggering observed in Southwest Japan	
<i>3.3.1</i>	<i>Seismicity activation following the 2011 <math>M_w</math> 9.0 Tohoku-oki earthquake</i>	36
<i>3.3.2</i>	<i>Evidence of triggering potential by both surface waves from the 2008 <math>M_w</math> 7.9 Wenchuan earthquake</i>	42
<b>3.4</b>	Conclusions	47
<b>Chapter 4</b> Decay characteristics of remote seismicity in Southwest Japan		
<b>4.1</b>	Introduction	49
<b>4.2</b>	Method and data	50
<b>4.3</b>	Short-term activation following the 2011 $M_w$ 9.0 Tohoku-oki earthquake	52
<b>4.4</b>	Activation at volcanic and non-volcanic regions	55
<b>4.5</b>	Fast-decay observed at volcanic regions in Kyushu, following the 2016 $M_w$ 7.3 Kumamoto earthquake	60
<b>4.6</b>	Conclusions	65
<b>Chapter 5</b> Discussion and conclusions		66
<b>Acknowledgements</b>		71
<b>References</b>		73

## **Abstract**

The concept of earthquake triggering is based on the understanding that the occurrence of an earthquake influences the shear and normal stress on surrounding faults. Static stress transfer by one earthquake on the surrounding crust may lead to follow-up earthquakes, while the passage of seismic waves in areas under critical conditions may result in failure of rock, slip on existing faults or pore pressure driven reactions in fluid related systems. The shaking produced by the surface waves at a certain location depends on many factors such as directivity, radiation, pattern and crustal structure (Chapter 1).

Seismic surface waves in particular seem capable of remotely trigger seismic activation in a variety of geodynamic events. My Ph.D. research is focused on systematically investigating remote triggering and mechanism responsible for triggering in SW Japan after the occurrence of two large earthquakes, the 2011 M9.0 Tohoku-oki earthquake and the 2016 M7.3 Kumamoto earthquake.

Firstly, I investigate triggering and the aftershock decay characteristics for the 2011 M6.4 Shizuoka earthquake sequence (Chapter 2). Next, I analyse the remotely activated seismicity in subduction regions like Aichi and Tokushima prefectures, in active faults environments like Tottori, Hyogo and Fukuoka prefectures, respectively in geothermal/volcanic regions of Kyushu (Chapter 3 and Chapter 4). The goal is to understand how earthquakes are triggered by the arrival of Love and Rayleigh waves, but to also try to gain a deeper understanding of fundamental fault behaviour in these regions.

Chapter 2 highlights the triggering processes associated with the 2011 M6.4 Shizuoka earthquake sequence; the mainshock of the sequence occurred on March 15, close to Mt. Fuji. To improve the detection of smaller earthquakes, I have applied the Matched Filter Technique (MFT; Peng and Zhao, 2009) for the time interval from the Tohoku-oki earthquake until seven hours after the Shizuoka earthquake. As a result of the analysis, no foreshock activity was detected prior to the March 15 Shizuoka earthquake, which contrasts with other similar inland seismicity activations following the Tohoku-oki. The early aftershock detection for the first 7 hours following the M6.4 event was significantly improved. When looking at the space-time distribution of the MFT detections, I observed that the earliest aftershocks (first minutes after the Shizuoka earthquake) occur to the north, close to Mt. Fuji, likely due to a stress increase from the Shizuoka mainshock. The largest earlier aftershocks ( $M \geq 4.0$ ) occur as well in the north region. The aftershock distribution and the focal mechanism data suggest that the northernmost earthquake may have occurred on a different fault segment. I also detect a rapid decay of aftershocks for this sequence, which may be related to a fast stress relaxation nearby high temperature magmatic reservoir.

In Chapter 3, I conduct a systematic search of remote seismicity activation in SW Japan, after the 2011 Tohoku-oki earthquake.. The results suggest the arrival of larger amplitude Love waves may correlate better with the occurrence of first locally triggered events compared to the Rayleigh wave arrivals. Based on the analysis of an extended earthquake catalogue, in Chapter 4, I show that the stacked seismicity for the dynamically triggered regions in SW Japan after the 2011 Tohoku-oki earthquake has a significant, but weak increase after the megathrust event, followed by a relatively slow decay towards the background level for the next several days. The relatively slow decay

may reflect the temporal pattern of stacked, swarm-like clustered seismicity, which has been mainly activated at volcanic/geothermal areas in Kyushu. The decay of seismicity within a single, activated earthquake cluster may have, however, different characteristics. The analysis of the aftershocks initiated dynamically at the Yufuin-Beppu geothermal area (Kyushu), by the 2016 M7.3 Kumamoto earthquake, shows a fast decay that may reflect quick stress recovery near higher-temperature volcanic or geothermal regions.

I discuss the observations and their implications in Chapter 5. The same rapid aftershocks decay from around Aso volcano was also observed in the other studied area, in Shizuoka region, around Mount Fuji. Although the triggering mechanism for this earthquake generation was challenging to identify due to the time delay, the fast aftershock decay indicates fast stress relaxation associated with high heat-flow values.

Dynamic triggering studies may help to estimate seismic hazards by further understanding and identifying near-critical conditions on faults through remotely triggered earthquakes. The short-term process that leads to slip nucleation and generation of earthquakes needs a better understanding and observations made in this study may enhance our knowledge about the variation in triggering behaviour and aftershock decay characteristics.

Key words: remote triggering, aftershock decay, Love and Rayleigh triggering potential, 2011 M9.0 Tohoku-oki, 2011 M6.4 Shizuoka earthquake, 2016 M7.3 Kumamoto earthquake, subduction regions, active fault regions, volcanic and geothermal regions.

## List of figures

### Chapter 2

<b>Figure 1.</b> Seismicity observed close to Mt. Fuji.	14
<b>Figure 2.</b> Time vs. magnitude distribution of the 2011 Shizuoka sequence from JMA catalogue.	15
<b>Figure 3.</b> Continuous waveform data from 7 Hi-net stations for horizontal and vertical components (NIED).	16
<b>Figure 4.</b> . Template event recorded at TU2H station for a M3.2 earthquake from 2011/03/15 22:33:35.	17
<b>Figure 5.</b> Cross-correlation between template and waveform-data.	18
<b>Figure 6.</b> New detection of an event by MFT.	19
<b>Figure 7.</b> Aftershock temporal decay of Shizuoka sequence.	20
<b>Figure 8.</b> Seismicity detected by MFT procedure.	22
<b>Figure 9.</b> Spatiotemporal aftershock distribution for JMA events and MFT detections.	24
<b>Figure 10.</b> Slip model of Shizuoka earthquake from JMA.	25
<b>Figure 11.</b> Spatio-temporal distribution of MFT detection and focal mechanism.	27
<b>Figure 12.</b> Heat flow map around Mt. Fuji.	28

### Chapter 3

- Figure 1.** Distribution of the seismic activity in Japan for the first 30 minutes after the 2011  $M_w$  9.0 Tohoku-oki earthquake (2011/03/11 14:46:18.12 JST). 37
- Figure 2.** Correlation between the remote earthquake triggering in Southwest Japan and the arrival of surface waves from Tohoku-oki mainshock. 39
- Figure 3.** Amplitude spectra of surface waves in Kagoshima, at YKWH station. 42
- Figure 4.** Remotely triggered areas in Kyushu by the 2008/5/12 15:28:01 (JST)  $M_w$ 7.9 Wenchuan earthquake. 44
- Figure 5.** Correlation between the remote triggering in Kyushu and the arrival of surface waves from the 2008 Wenchuan earthquake. 45

### Chapter 4

- Figure 1.** Areas in Southwest Japan with observed dynamic triggering by the 2011 Tohoku-oki earthquake. 51
- Figure 2.** Temporal evolution of seismicity before, during and after the remote triggering activation. 53
- Figure 3.** Seismicity observed at subduction interface areas for 60 days before and after Tohoku-oki earthquake. 56
- Figure 4.** Seismicity observed at active fault areas for 60 days before and after Tohoku-oki earthquake 57

<b>Figure 5.</b> Seismicity observed in the volcanic regions in Kyushu for 60 days before and after Tohoku-oki earthquake.	58
<b>Figure 6.</b> Spatial distribution and temporal decay for the 2016 Kumamoto aftershock sequence.	61
<b>Figure 7.</b> Aftershock spatial distribution and temporal decay for the 2016 Kumamoto sequence.	63
<b>Figure 8.</b> Heat flow map around Aso and Yufuin-Beppu volcanic regions.	64

## **Chapter 5**

<b>Figure 1.</b> Maximum dynamic stress changes due to the passing of surface waves from the 2011 Tohoku-oki earthquake.	67
<b>Figure 2.</b> Triggering model for observed seismicity in SW Japan.	68

## **List of tables**

### **Chapter 3**

<b>Table 1.</b> The catalogue of early triggered events in Southwest Japan, following the 2011 M9.0 Tohoku-oki earthquake.	34-35
<b>Table 2.</b> Teleseismic events from the ANSS catalogue	43

# Chapter 1

## Introduction

### 1.1 Background: earthquake triggering mechanism

The concept of earthquake triggering is based on the understanding that the occurrence of an earthquake influences the shear and normal stress on surrounding faults. As discussed by King et al. (1994) and Stein (1999), even a small, sudden stress change can cause large changes in seismicity rate. The areas associated with stress increase are known to have a higher rate of seismic activity and are usually described as aftershock areas, while the areas where the stress drops have a lower seismicity rate. It was observed that both increases and decreases in seismicity rate are followed by a time-dependent recovery to background seismic activity.

Earthquake triggering mechanism was described in relation with stress change. Static or permanent stress transfer from source to receiver fault is referred as static triggering, while transient stress change due to the passage of surface waves from large earthquakes represents dynamic triggering.

Static stress transfer by one earthquake on the surrounding crust may lead to follow-up earthquakes. As King et al. (1994) shows for the 1992 Mw 7.3 Landers earthquake, the slip resulted in a change of the regional stress field and lead to the triggering of subsequent earthquakes, according to Coulomb failure criterion, which states that aftershocks are abundant where the Coulomb stress on optimally orientated faults increases, and aftershocks are sparse where the Coulomb stress drops.

Coulomb failure stress change ( $\Delta CFS$ ) can be expressed using the following relationship:

$$\Delta CFS = \Delta\sigma_f = \Delta\tau + \mu'\Delta\sigma_n$$

where  $\Delta\tau$  is the shear stress change on a fault (positive in the direction of fault slip),  $\Delta\sigma_n$  is the normal stress change (positive if the fault is unclamped) and  $\mu'$  is the apparent friction coefficient (with range  $0\pm 1$ ). The parameter  $\mu'$  is intended to include the effects of pore fluids as well as the material properties of the fault zone (Harris, 1998).

Using this approach, Stein et al. (1997) presents an impressive earthquake prediction study, demonstrating in retrospective the progressive failure since 1939 of the North Anatolian fault, Turkey, by static stress transfer. The mechanism also applies to volcanic systems, where the static reduction of normal stress may trigger magma ascent which eventually results in a volcanic eruption (Nostro et al., 1998; Marzocchi et al., 2002).

The static stress changes decay with distance ( $r$ ), approximately proportional to  $r^{-3}$ , for distances exceeding the source extent (Aki and Richards, 2002), while the dynamic stress changes attenuate much slower (as  $r^{-3/2}$ , for surface waves, Hill et al., 1993). As documented from many observations, the static stress transfer it is only effective within regional distances, which are up to approximately one fault length from the triggering earthquake (Hill and Prejean, 2006). This limits the range of static stress triggering to several hundred kilometers even for large  $M_w > 8$  earthquakes.

Hill et al. (1993) reported a sudden and widespread increase in earthquake activity across much of the western United States following the 1992  $M_w$  7.3 Landers earthquake. Triggered earthquakes occurred up to 1250 km from the mainshock and

could not be explained by static stress transfer. He argued that the increase of seismicity was remotely triggered by the dynamic stresses accompanying transient seismic waves. The 1992 Landers, California earthquake demonstrated that the triggering capability of earthquakes can extend far beyond regional distances as expected from static stress triggering.

Therefore, in general, activated seismicity that occurs at more than a few lengths from the mainshock could be attributed to dynamic rather than static stress changes, since the last ones become negligible. The shaking produced by the surface waves at a certain location depends not only on the distance between the source and receiver, but also on other factors such as directivity, radiation, pattern and crustal structure (e.g., Manga and Brodsky, 2006).

During the passage of seismic waves, the ground is temporarily subject to additional stresses which under critical conditions may result in failure of rock, slip on existing faults or pore pressure driven reactions in fluid related systems. Seismic surface waves in particular seem capable of remotely trigger seismic activation in a variety of geodynamic events, both immediately and during the passage of the waves or delayed by hours to days (Brodsky, 2006).

The physical models used to explain the triggering by dynamic stresses proposed by Hill and Prejean (2006):

(1) direct triggering by frictional failure, where dynamic stresses provide the necessary stress increase to exceed the frictional strength of faults; the model can be applied in regions where faults are close to failure and oriented with respect to the polarity of the dynamic stress caused by distant large earthquakes.

(2) triggering through excitation of crustal fluids due to fluid transport and pore pressure changes; in active geothermal areas, pore pressure redistribution might be a significant triggering mechanism.

## 1.2 Review of decay characteristics of earthquakes

Temporal behaviour of aftershocks has been adopted to study relationship between the mainshock and aftershocks (Peng et al. 2006; Enescu et al. 2007). The decay of aftershocks over time follows a power law relationship known as Omori's Law (Omori, 1894):

$$N(t) = \frac{K}{(c + t)},$$

where  $t$  represents the time from the occurrence of the mainshock and  $N(t)$  is the frequency of aftershocks in given time interval.

However, a modified Omori law (Utsu 1961) fits the occurrence rate of aftershocks better:

$$N(t) = \frac{K}{(c + t)^p},$$

The exponent  $p$  reflects the decay rate of the aftershock sequence, where  $p$  has a value generally close to 1, but variable for different locations. Values greater than 1 would have relatively rapid decay rates and values less than 1 would have relatively slower decay rates.

$K$  is the aftershock productivity depending on total number of events in the aftershock sequence and  $c$  is the constant time shift introduced to avoid singularity when  $t$  goes to 0. To determine these parameters, the most commonly used method is maximizing the logarithm of the likelihood function described by Ogata (1983).

Omori law with  $p$ -value of 1 can be predicted from the state and rate friction law (Dieterich, 1994). The physical significance of  $c$  value is still under debate, mostly because it is difficult to determine early aftershock events after the main shock (Kagan 2004).

The aftershock decay described by the  $p$ -value from the Modified Omori Law can vary from 0.8 to 1.5, regardless of the cut-off magnitude, depending on fault heterogeneity (Mikumo and Miyatake, 1979; Yamashita and Knopoff, 1987; Nanjo et al., 1998), heat flow, stress and temperature in the crust (Mogi, 1962; Kisslinger and Jones; 1991; Utsu et al., 1995). Although, it is not clear which of these factors has the largest influence on the variation of  $p$ -value, a strong dependence between the distribution of stress relaxation times and  $p$ -value was observed (Kisslinger and Jones, 1991). Large  $p$ -value can be associated with short relaxation time and large rate of recovery of the fault strength.

Existing catalogues are usually used in previous studies on aftershock decay rate (Utsu et al., 1995). However, it has been known that existing catalogues are not complete for early aftershocks occurred in a short period time after the mainshock, either due to overlapping of coda waves of large events or overwhelmed network analyst by too many events (Kagan 2004). To study early aftershock rate, detailed waveform analysis is usually necessary.

### 1.3 Research purpose and objectives

Triggering associated with the occurrence of large earthquakes was studied by many authors in many different regions of the world. Theoretically, the mechanism of earthquake triggering in the vicinity of faults or at large distances from the source are very well described. Nevertheless, depending on local or regional conditions, sometimes it might very difficult to distinguish between different triggering causes.

I would like to understand the complex mechanism associated with the occurrence of the delayed M6.4 Shizuoka earthquake by investigating the seismicity activation in the region after the 2011 M9.0 Tohoku-oki earthquake. Based on seismic observations can the understanding of local conditions that contribute to earthquake triggering be improved?

The dynamic triggering of seismicity at remote locations by the passage of surface waves from large earthquakes is a well-documented phenomenon. Somewhat surprisingly, remote activation of earthquakes in Japan is relatively scarce (Brodsky, 2006) before 2011, despite high-levels of seismicity associated with active faulting and volcanism.

There are two notable cases of triggered seismicity activation in Japan: the 2011 Tohoku-oki earthquake (Toda et al., 2011, Enescu et al., 2012, Miyazawa 2011, Shimojo et al., 2014) and the 2016 Kumamoto earthquake (Enescu et al., 2016, Miyazawa 2016).

The physical mechanisms responsible for the remote activation of seismicity are still poorly understood. Two main classes of models have been proposed by Hill and Prejean (2015) to explain the triggering by dynamic stresses: (1) direct triggering by frictional

failure and (2) triggering through excitation of crustal fluids. Can these mechanisms be used to explain the triggering observed in SW Japan after the occurrence of the 2011 Tohoku-oki earthquake?

By analysing the seismicity activation in SW Japan, in different tectonic regions, like subduction area, active fault environments or volcanic and geothermal regions, I aim to explain different seismicity features observed, in relation with their physical meaning.

## Chapter 2

### Triggering of the 2011 M6.4 Shizuoka earthquake sequence

#### Abstract

Many inland areas in Japan were seismically activated following the 2011 M9.0 Tohoku-oki earthquake. The activation mechanism includes triggering by dynamic, static or fluid-induced stress changes (e.g., Toda et al., 2011; Miyazawa et al., 2011; Shimojo et al., 2014). In this study I aim to understand the triggering processes associated with the 2011 M6.4 Shizuoka earthquake sequence; the mainshock of the sequence occurred on March 15, close to Mt. Fuji. To improve the detection of smaller earthquakes, I have applied the Matched Filter Technique (MFT; Peng and Zhao, 2009) for the time interval from the Tohoku-oki earthquake until seven hours after the Shizuoka earthquake. I used Hi-net (NIED) continuous waveform data and seismograms of 1126 template events with  $M \geq 1.0$ , which occurred in the study area between 2001 and 2014. The total number of Hi-net stations used was 25, selected within a 40 km radius from the main shock. No foreshock activity was detected prior to the March 15 Shizuoka earthquake, which contrasts with other similar inland seismicity activations following the Tohoku-oki earthquake (e.g., Kato et al., 2013; Shimojo et al., 2014). Since the co-seismic static stress change due to the Tohoku-oki earthquake on the Shizuoka fault plane was significant ( $\sim 0.5$  bar), one can argue that this is likely the most significant triggering mechanism and the delay of this sequence could be explained by the rate-and-state friction law (Dieterich, 1994). The aftershock detection for the 7 hours following the M6.4 event was significantly improved. When looking at the space-time distribution of the MFT detections, I observe that the earliest aftershocks (first minutes

after the Shizuoka earthquake) occur to the north, close to Mt. Fuji, likely due to a stress increase from the Shizuoka mainshock. The largest earlier aftershocks ( $M \geq 4.0$ ) occur as well in the north region. Aftershock distribution and focal mechanism data suggest that the northernmost earthquake may have occurred on a different fault segment. I also detected a rapid decay of aftershocks for this sequence, which may be related to a fast stress relation nearby high temperature magmatic reservoir.

## 2.1 Introduction

Earthquake-earthquake interactions in the form of mainshock-aftershock sequences have been well recognized for many decades. Stress changes resulting from one earthquake are capable of triggering additional earthquake activity over a surprisingly wide range of distances and time scales. As currently understood, earthquake interactions are generally placed under one of three rather general stress transfer modes: static, quasi-static, or dynamic (Hill and Prejean, 2006).

Triggering can occur when the stress state on a fault temporarily exceeds the rupture threshold. Static triggering is based on the idea that permanent stress transfers from a source to a receiver fault. This stress change is produced by the dislocation of a seismic fault but is effective only in the region close to the fault, since the magnitude of stress change attenuates by  $1/r^3$ , where  $r$  is the distance from the earthquake fault.

Quasi-static stress change is caused by the viscoelastic relaxation of the lower crusts and the upper mantle around the earthquake fault. Quasi-static stress changes propagate as a two dimensional stress change, thus it decays more slowly with distance, by  $1/r^2$ .

The triggering potential extends to greater distances than static stress changes, and the relatively low viscoelastic propagation speed results in delayed triggering (Pollitz and Sacks, 2002).

Dynamic triggering of earthquakes has been widely observed due to the passage of surface waves from large earthquakes. Usually, the transient stress and triggering effect vanishes after the passage of seismic waves or in a short time after. The amplitudes of dynamic stresses propagating as seismic waves decrease relatively slowly with distance (as  $1/r^2$ , for body waves and  $1/r^{3/2}$ , for surface waves), and thus, their triggering potential extends from the near-field to much greater distances than either the static or quasi-static stress changes (Hill and Prejean, 2006).

In this study I investigate the triggering mechanism of a magnitude 6.4 event which occurred close to Mt. Fuji, 4 days after Tohoku-oki, at a distance of about 500 km from the mainshock. Since the Tohoku-oki rupture area extended over 400 km in length (Yagi and Fukahata, 2011), it can be considered that the amplitude of both static and dynamic stresses is significant to trigger seismicity in the Shizuoka area.

Mount Fuji is a famous stratovolcano located near the junction of three tectonic plates: the North American plate, the Eurasian Plate and the Philippine Sea Plate. This complex tectonic environment gives Mount Fuji some unique chemical variations (basaltic eruptions during the last 100.000 years) due to fractional crystallization of a hydrous magma in a deep magmatic chamber Fujii (2007), located at depths of 15-25 km.

These observations are also sustained by recent deep low frequency (DLF) seismic swarm activity (Nakamichi et al., 2007). In a more recent paper, Kaneko et al (2010), proposed the existence of at least another shallower magmatic chamber that is situated

at depths of around 10 km and has a more SiO<sub>2</sub> rich component than the deeper basaltic one.

It is notable that before the occurrence of the 2000 and 2001 DLF seismic swarm events, which occurred shortly after the eruption of Miyakejima volcano, no significant seismic activity or crustal deformations, were observed in the area (Ukawa, 2005). This lack of seismicity and geodetic activity continued to be observed until the occurrence of the Shizuoka main event.

As mentioned before, both static and dynamic stress changes induced close to Mount Fuji have similar effects, with the difference that the dynamic influence can be observed only during the passage of surface waves, or shortly after. Although the static triggering process can result in a delay of seismicity activation, this phenomena doesn't have any clear patterns.

After the occurrence of the Shizuoka sequence, static stress changes on Shizuoka fault plane were calculated by Toda et al. (2011) and Enescu et al. (2012) and the obtained values are around 0.5 bar, value that is above the threshold of inducing static triggering.

Fujita et al. (2013) investigated the stress field changes around Mount Fuji magmatic system, in order to estimate a potential eruption. The static stress changes calculated using finite element method were around 0.01-0.1 bar at the boundary region between the magma reservoir and the surrounding rocks.

Aizawa et al. (2016), based on a joint three-dimensional resistivity and isotopic analysis of the ground water system in the area, proposes the triggering of the Shizuoka sequence due to shaking by seismic waves which induced the upwelling of fluids

through fracture pathways. The resulting model shows a pore pressure increase of about 100 bars, capable of generating the Shizuoka main event.

Considering the dynamic triggering hypothesis, a complete earthquake catalog is required to offer more insights into the seismic activity following the passage of the surface waves from the 2011 Tohoku-oki earthquake. Thus, I explain in the next chapter the use of the waveform based method to improve the catalogue completeness. Based on seismicity observations, I will try to elucidate the triggering mechanism responsible for this earthquake generation.

## **2.2 Method and data**

On March 15, 2011, at 22:31:46.34 JST (local time) a 6.4 magnitude earthquake occurred beneath the south flank of Mountain Fuji, just above the magma system. It occurred with a 4 days delay from the megathrust event (March 11, 14:46 JST) and was located about 500 km SW of the Tohoku megathrust fault (Figure 1a).

First, I used the data recordings from a network that operates under NIED and it is installed around active volcanic regions in Japan. The V-net seismic stations are conveniently located around Mountain Fuji, but unfortunately, due to many power failures caused by the megathrust event, only FJSV station was completely operational at the time of the magnitude 6.4 earthquake occurrence. I used this station to manually inspect the waveform data searching for the possibility of locally triggered earthquakes associated with the arrival of surface waves from the megathrust event. I could not find any evidence for instant activation, thus I decided to apply a systematic search for any

earthquakes that might have occurred in the 4 days interval between the two earthquakes mentioned before.

For this study I used three-component continuous waveform data recorded at 25 seismic stations on a 30 km radius around Mountain Fuji (Figure 1b). The waveforms and the catalogue were provided by the Japanese High Sensitivity Seismograph Network (Hi-net), operated by the National Research Institute for Earth Science and Disaster Prevention (NIED).

The time interval for which I analysed the continuous waveform data begins after the occurrence of the M9.0 Tohoku-oki Earthquake, on 11 March 2011 and ends 7 hours after the occurrence of the main local event, which I will call from now on Shizuoka Earthquake, on 15 March 2011.

Besides continuous waveform recordings, I also used earthquake catalogue data provided by Japan Meteorological Agency (JMA), for the time interval between 2001 and April 30, 2011.

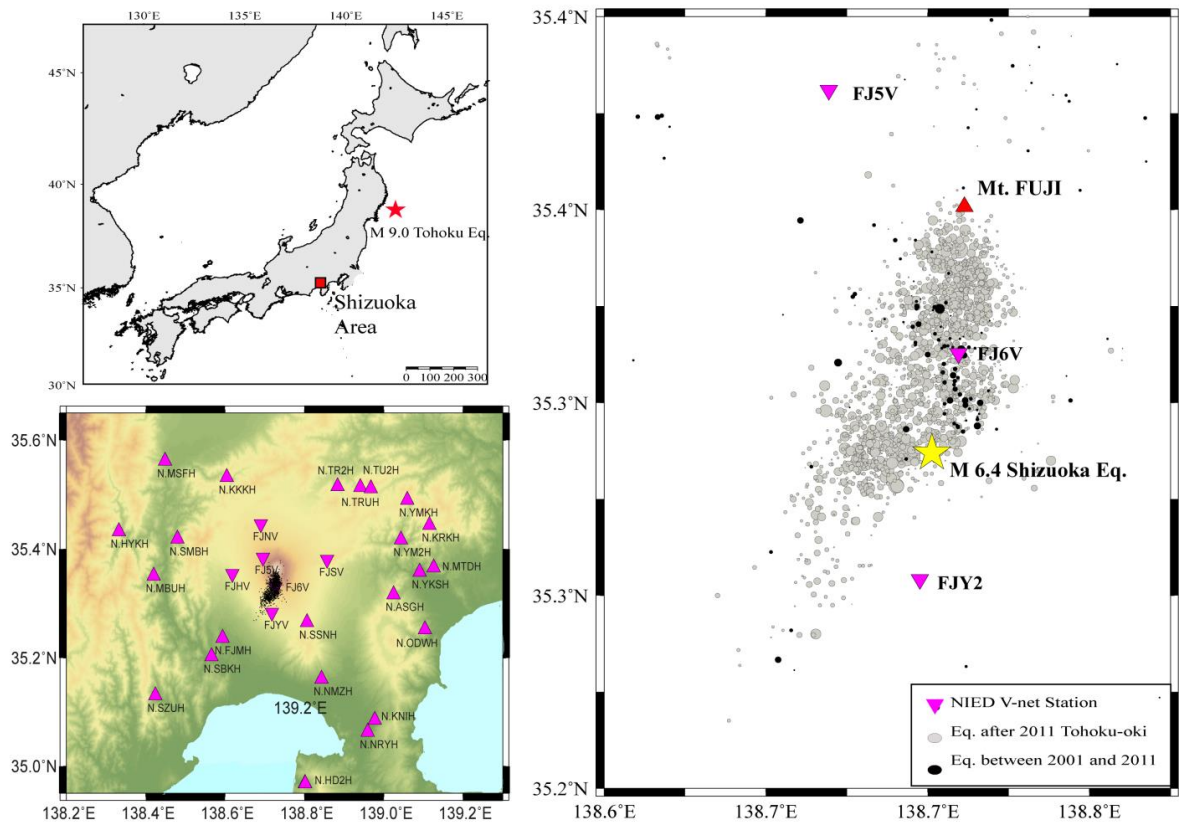


**Figure 1. Seismicity observed close to Mt. Fuji.** a) Shizuoka mainshock area (red square) and Tohoku-oki earthquake (red star) plotted on Japan map. b) Station distribution around study area. Purple triangles show the Hi-net stations, while the upside down triangles shows V-net stations. c) Seismicity around Mt. Fuji (red triangle) from the JMA catalogue. Black circles represent the events between 2001 and 2011 Tohoku-oki earthquake, while the grey ones are JMA detections after 2011 Tohoku-oki. The yellow star shows the main event of the Shizuoka sequence that occurred on March 15 2011, 21:31:46.34 (JST).

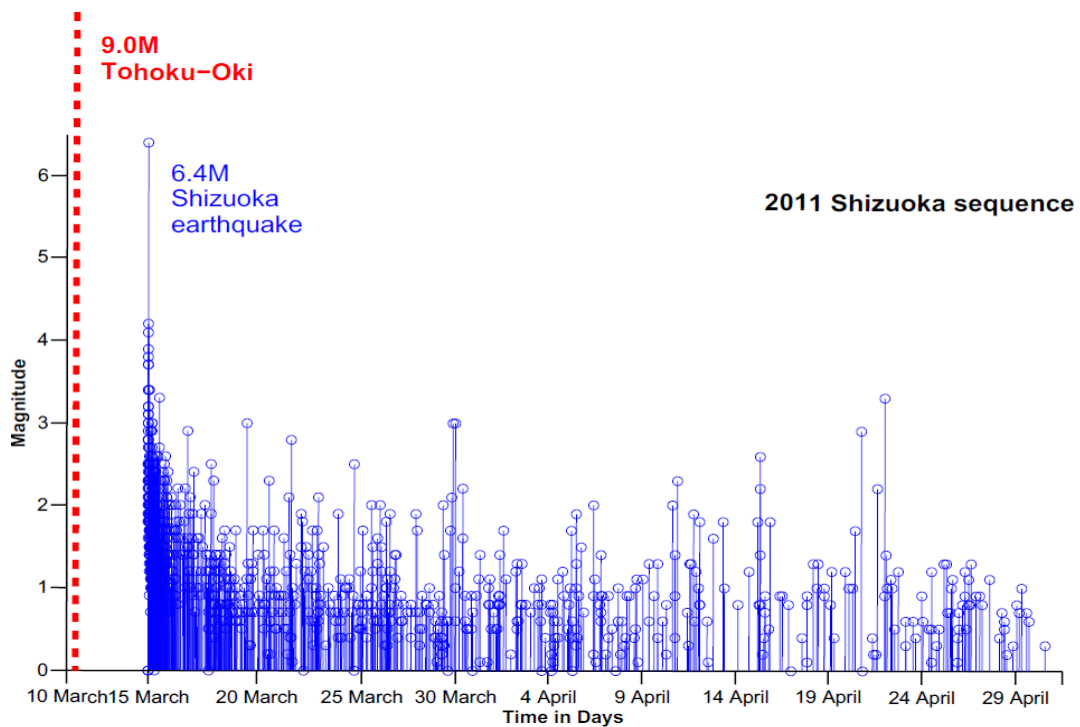
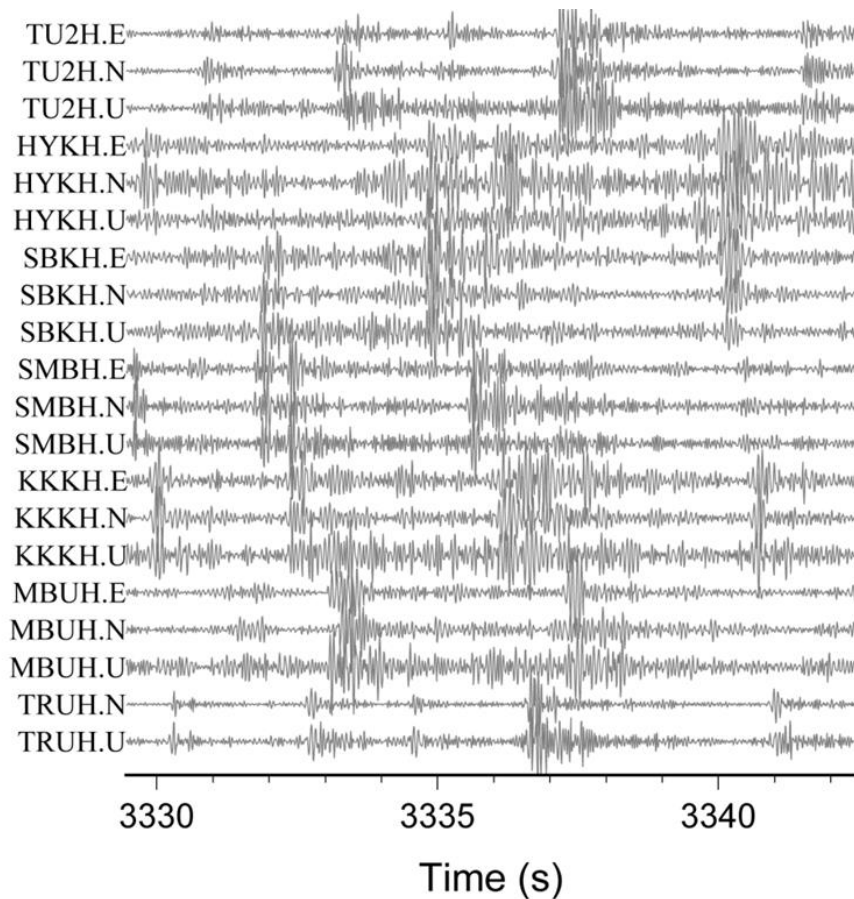


Figure 2. **Time vs. magnitude distribution of the 2011 Shizuoka sequence from JMA catalogue.** The interval between Tohoku-oki and Shizuoka main event shows a seismicity gap that might reflect hidden seismicity due to the occurrence of the megathrust event.

I notice that the JMA catalogue has no detected events in the time interval between the occurrences of the two earthquakes (Figure 2). Thus, in order to detect earthquakes that are usually hidden by the mainshock coda-wave or by overlapping earthquakes and which might be missing from the Japanese Meteorological Agency (JMA) catalogue, I have applied a waveform-based method known as Matched Filter Technique.

The number of selected template events, from the Hi-net catalogue, with magnitude larger than 1.0, which occurred between March 2001 and December 2014, was 1126 (Figure 1c).

I used these templates to search through the continuous recordings, such as those shown in Figure 3, in order to detect seismic events by waveform cross-correlation. Both the continuous waveforms and the templates were filtered by a two-way 10-30 Hz Butterworth Bandpass filter. Such a filtering ensures a good detection of local events.



**Figure 3. Continuous waveform data from 7 Hi-net stations for horizontal and vertical components (NIED).** Recordings showing a 13 seconds time interval, after March 15, 2011 22:30:00.

I selected a 4 seconds time window for each template event recorded, starting 2 seconds before the arrival time of the S-wave, as seen in the template event recorded at TU2H station (Figure 4). If the signal-to-noise ratio (measured as the average waveform amplitude from -6 seconds to -2 seconds before P wave arrival) was larger than 5, I used it in the next step. By shifting the time window with an increment of 0.01 seconds through the continuous waveforms, I computed the correlation coefficient between the template events and the continuous recordings. At each time point, the correlation coefficient value was assigned to its origin time by subtracting the computed S-wave arrival time.

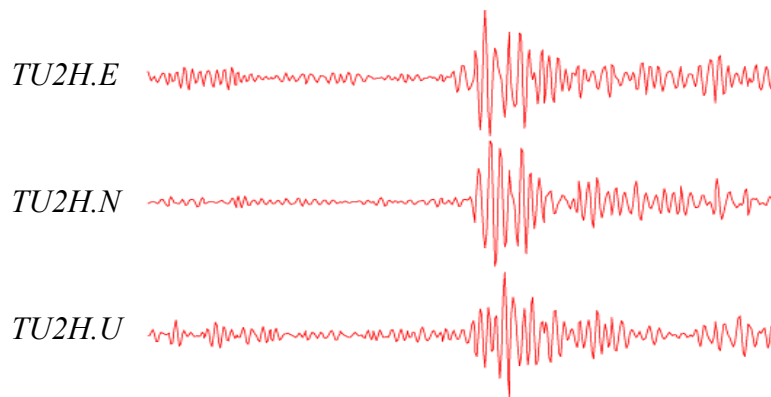


**Figure 4. Template event recorded at TU2H station for a M3.2 earthquake.** The origin time of this aftershock is 2011/03/15 22:33:35.

For the next step, I stacked the correlation coefficient values for all stations at the three components and compute the mean correlation coefficient value at each time point (Figure 5a). The stacking allows us to measure the similarity between the template and newly detected events.

Next I use a statistical test and compute the median absolute deviation (MAD) for the mean correlation coefficient trace for each template event. If the value is over the detection threshold, which in this case is nine times the MAD, I consider I have a new detected event (Figure 5b). The chance of random detection using this threshold is about one event per day (Peng and Zhao, 2009).

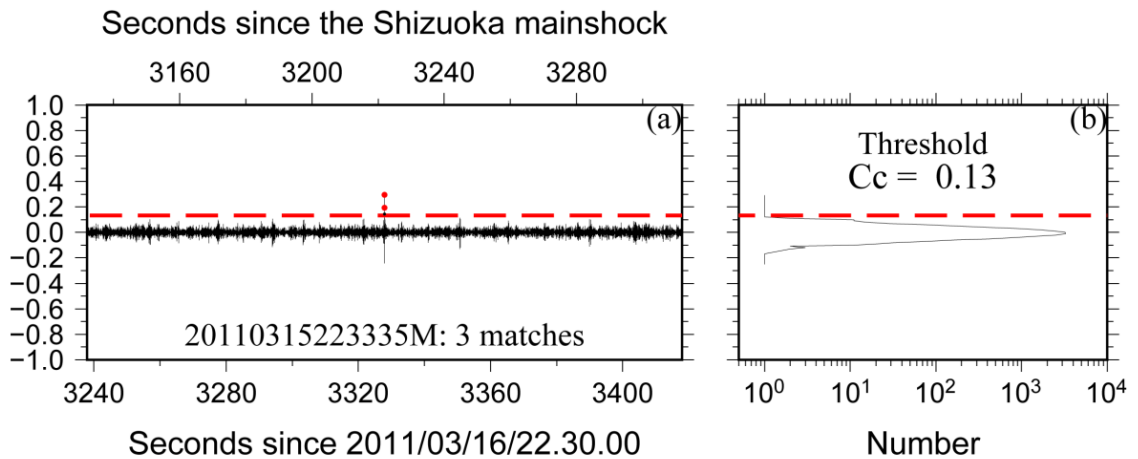


**Figure 5. Cross-correlation between template and waveform-data.** (a) Mean cross-correlation time series between one template-event and the continuous waveform data; the discontinuous line indicates the threshold used for event-detection; the pick-value indicated by a small full circle corresponds to a detected event. (b) Histogram of the mean cross-correlation coefficients;

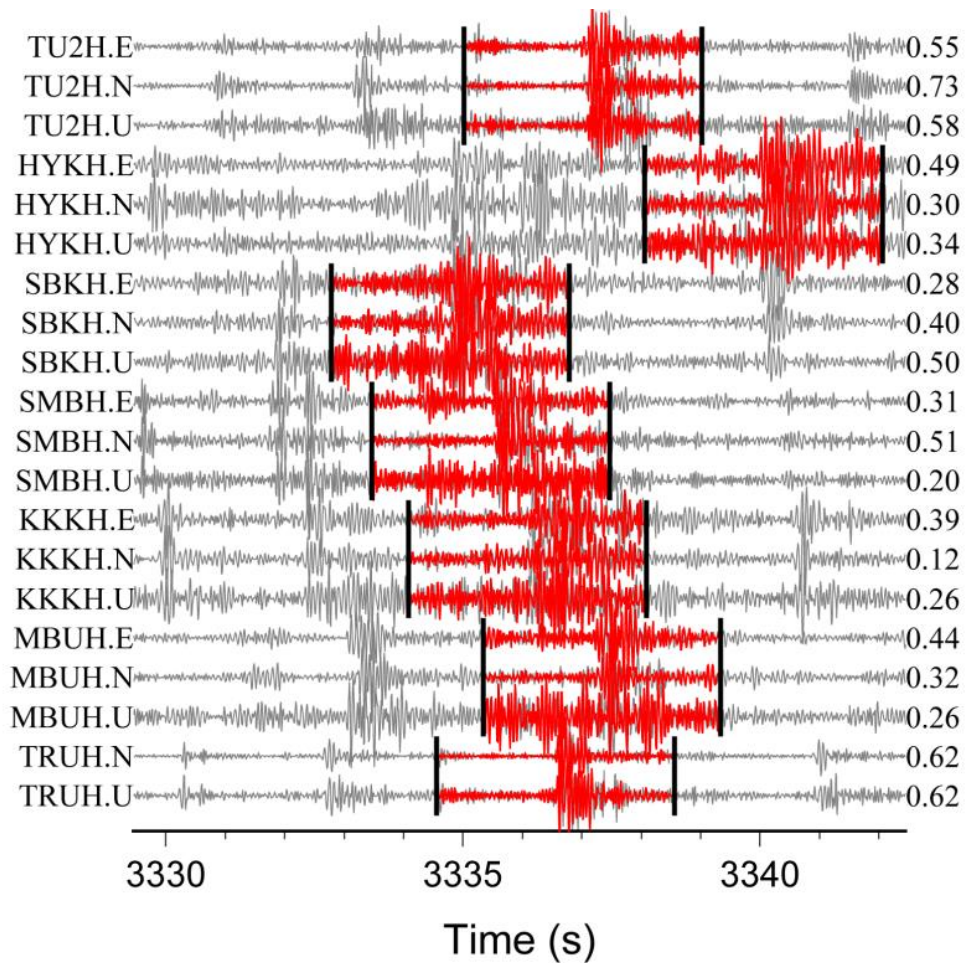


**Figure 6. New detection of an event by MFT.** Comparison between a template event (red) and continuous waveforms (grey) at Hi-net stations (the average cross-correlation coefficient for this detection is 0.3) for a newly detected event with magnitude of 2.4.

Because the newly detected events have similar waveforms with the template event, I assigned the location of the new events with that of the corresponding template. The origin time of the detected event is the time associated with the highest mean correlation coefficient value, while the magnitude was estimated based on the median value of the maximum amplitude ratios for all channels between the template and detected events, assuming that a tenfold increase in amplitude corresponds to one unit increase in magnitude (Figure 6).

For analysing the decay characteristics of this sequence, I combine the MFT detections for early aftershocks and the JMA catalogue. The magnitude of completeness is above 1.5. Using the maximum likelihood function (Ogata, 1983), I obtain the Modified Omori-fit to the data (Figure 7).

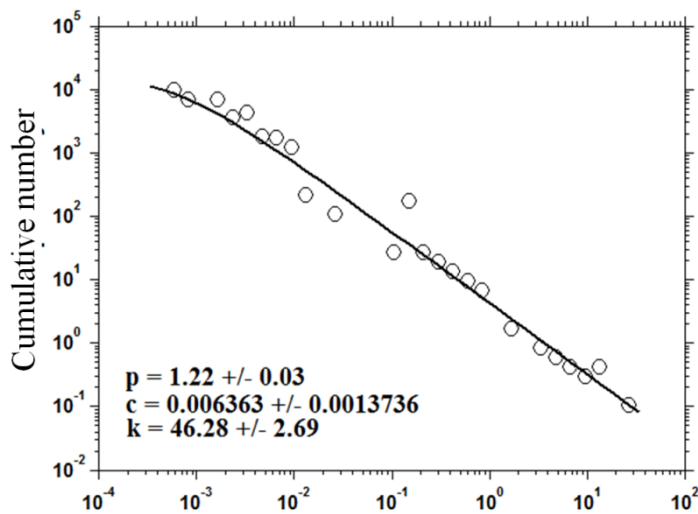


**Figure 7. Aftershock decay of Shizuoka sequence.** In the cumulative number to time plot the line represents the Modified Omori Law fit for the combined catalogue of the Shizuoka sequence, in the time interval between 2011/03/15 and 2011/04/30, for a magnitude of completeness  $M_c > 1.5$ .

## 2.3 Results and discussions

When trying to understand the triggering mechanism of the 2011 M6.4 Shizuoka earthquake, it is important to have a clear picture of the seismicity. Since the mainshock occurred four days after the megathrust M9.0 Tohoku-oki earthquake, I applied the MFT procedure to improve the catalogue completeness. Thus I obtained a new catalogue which I will discuss in the next section.

For the interval between Tohoku-oki and Shizuoka earthquake, the JMA catalogue presents no earthquakes recorded in the area. After checking the continuous waveforms at the closest stations operated by NIED (Hi-net and V-net networks) by manual inspection, I could not find any triggering associated with the arrival of surface waves from Tohoku-oki earthquake.

I have applied the MFT procedure for this interval and I only obtained two detections, just before the Shizuoka main-shock. At a close inspection of these two events, I realised that those were false detections, due to the fact that signal-to-noise ratio was very small and there were other overlapping Tohoku-oki aftershocks.

Further considering the dynamic triggering theory, which states that seismic waves from a large earthquake propagating through an area may increase the seismicity, if that area is close to failure (Hill et al., 1993), I decided to take a closer look at the waveform recordings following two Tohoku-oki aftershocks in Fukushima which occurred at a distance of about 400 km from Shizuoka earthquake.

I investigated manually the interval between 18:50:00 local time and the origin time of the Shizuoka main-shock. Two earthquakes occurred in March 15, 2011, a first M6.3 earthquake, at 18:49:51 local time, and a second M6.2 earthquake, just before the

Shizuoka event, at 22:27:53. When looking at the waveforms, I were not able to find any evidence of dynamically triggered local events from these particular aftershocks.

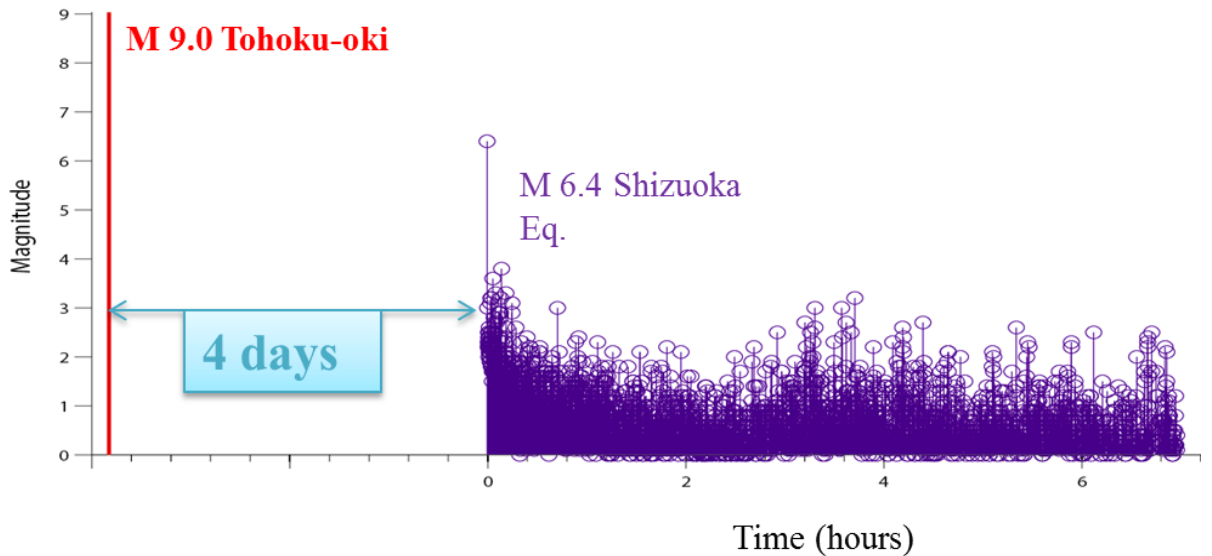
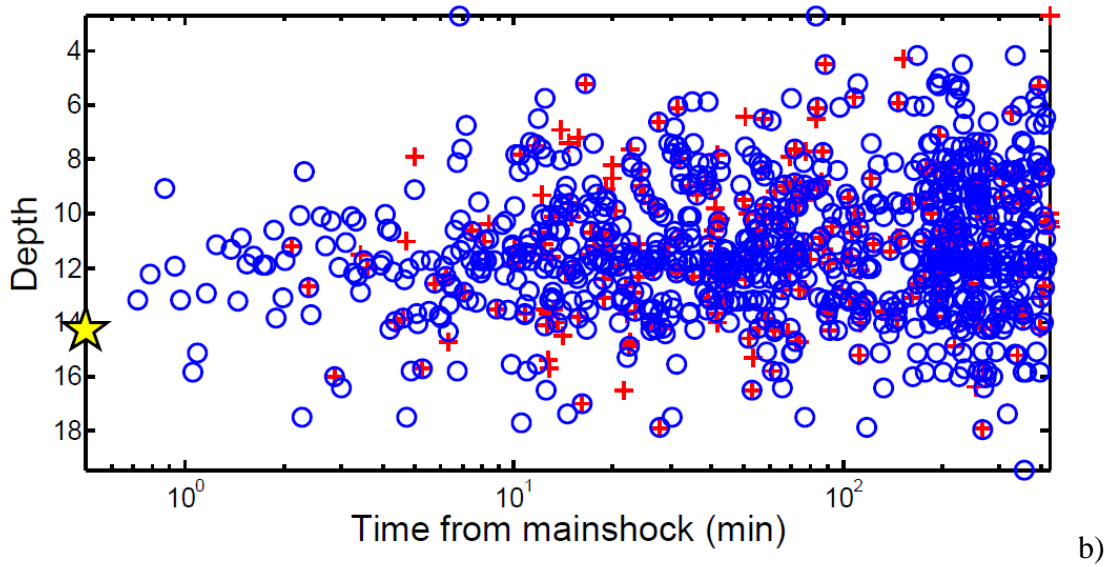
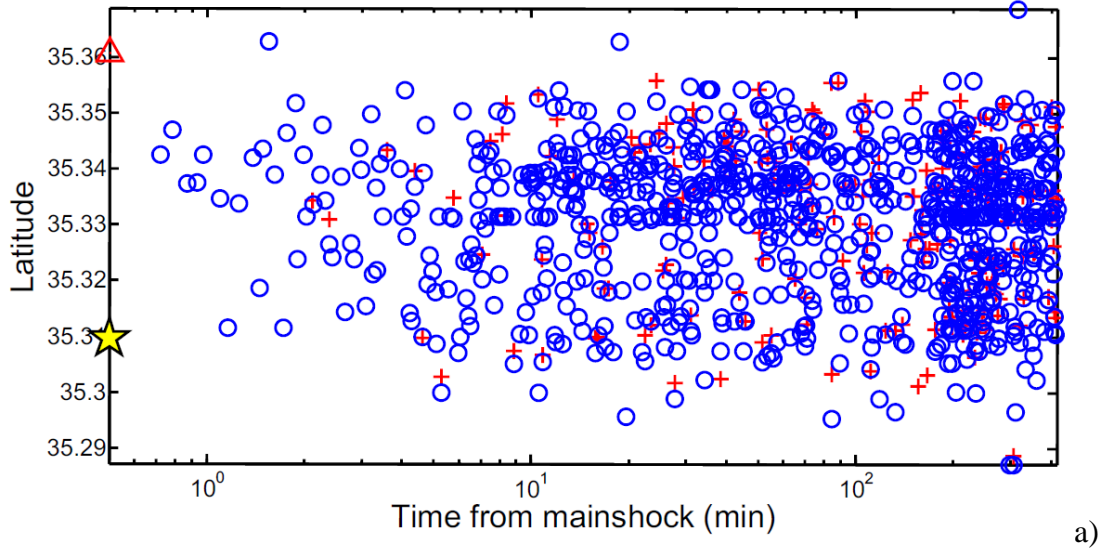


**Figure 8. Seismicity detected by MFT procedure.** For the 4 days interval between the two earthquakes, no seismicity was detected in the Shizuoka area.

Thus, I can conclude that before the occurrence of the M6.4 Shizuoka earthquake, the area did not experience any local seismic activity that can indicate dynamic triggering associated with the arrival of surface waves from the Tohoku-oki mainshock or any of its strong aftershocks.

After applying the MFT procedure for the aftershock sequence, the number of detected events increased about 14 times. The initial JMA catalogue contains 218 events for the first 7 h, while the new MFT catalogue has 3066 detected events for the same time interval. For further analysis I selected the events that have a magnitude greater than 1.0, the final number of selected events being 879.

The aftershock distribution seen in Figure 9 shows the comparison between the JMA catalogue (red) and the MFT detections (blue) or the first 7 hours since the occurrence of the Shizuoka mainshock.



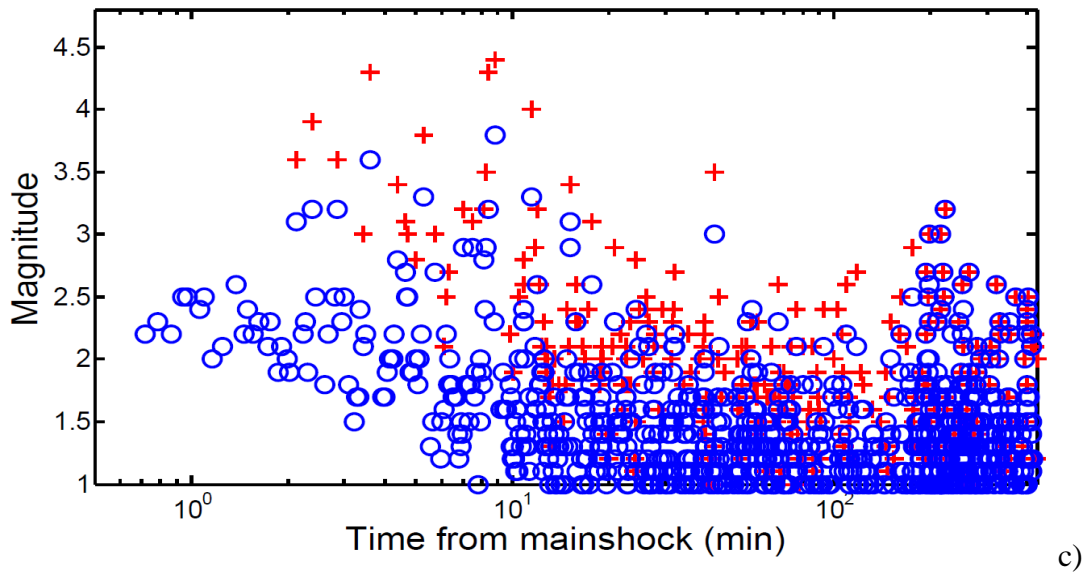


**Figure 9. Spatiotemporal aftershock distribution for JMA events and MFT detections.**a) Latitude to time plot b) Depth to time plot, respectively c) Magnitude to time for the JMA events (red cross) and MFT events (blue circle), 7 hours after the Shizuoka mainshock..

I compared the spatiotemporal distribution of early aftershocks of the Shizuoka sequence and observed that by applying the MFT procedure I improved the detection of early aftershocks, especially for the first 10 minutes after the main event.

I also notice the fact that the magnitude of the JMA detections is slightly larger than the one of MFT detections. This is due to the fact that the MFT magnitude was estimated only from high frequency components. I compute the peak amplitude ratio between template events and MFT detected events, assuming that a tenfold increase in amplitude corresponds to one unit increase in magnitude.

Next, I use the slip model provided by JMA for the Shizuoka earthquake (open access on the JMA webpage <http://www.data.jma.go.jp/svd/eqev/data/sourceprocess>). The cross section points are shown in red in topographic map view in Figure 9a. I represent the slip model obtained from JMA, using Nearest Neighbour interpolation method and overlay on top of the slip area the newly detected MFT aftershock hypocentre for different time intervals.

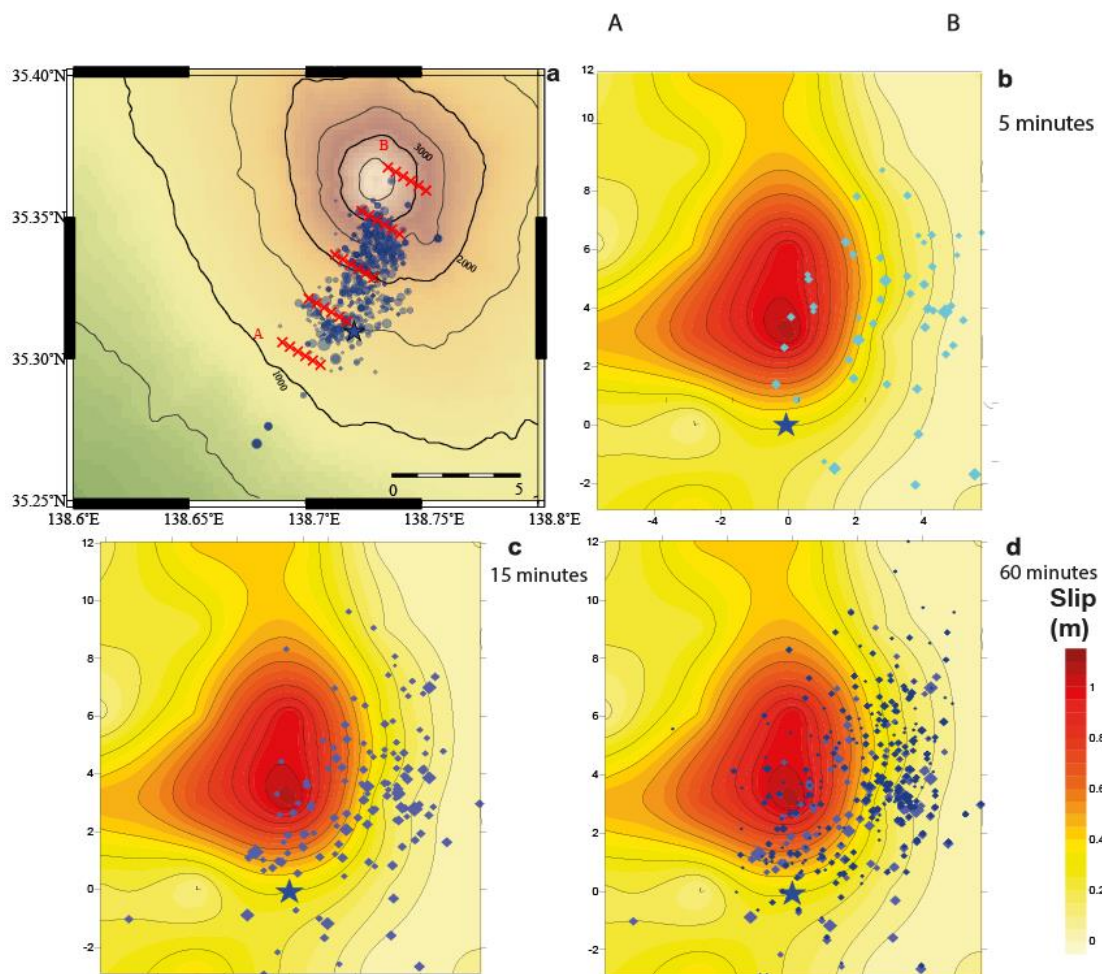


**Figure 10. Slip model of Shizuoka earthquake from JMA** a) Cross section grid points (red cross) and epicentre distribution (blue circles) around Mt. Fuji (from JMA slip model). Aftershock occurrence for the b) first 5 minutes after the main event; c) first 15 minutes; and respectively d) first hour of aftershock distribution.

As seen in Figure 10, aftershocks detected by MFT for the first five minutes after the occurrence of the main event seem to reflect a homogeneous distribution on the fault plane. Only a small number of events occur near the area of large slip values, while the mainshock occurs at the southern edge, away from the maximum slip area. For a wider time interval, of 15 minutes and respectively 60 minutes after the main event occurrence, the aftershocks hypocentre follow the same spatial distribution. This trend is observed throughout the spatiotemporal distribution of all MFT detections (Figure 11). Thus, we do not have any evidence of early aftershock area expansion, which might be a good indicator of fluid migration (Yamashita, 2003).

I also retrieved F-net CMT focal mechanisms from NIED (Figure 11b). The M6.4 Shizuoka main event and the surrounding aftershocks indicates a strike-slip mechanism, with an NW-SE dipping fault (strike  $29^\circ$  / dip  $82^\circ$  / rake  $20^\circ$ ). However, in the northern part, the mechanisms are more complex (like normal fault earthquake. that occurred in the first 10 minutes after the main shock). This suggests that there is some structural discontinuity in the northern part, close to Mount Fuji caldera.

As for the aftershock decay characteristics, I notice a relatively increased p-value for the Shizuoka sequence, which according to Dietrich's rate-and-state model (Dietrich, 1994), could be related to a non-constant stressing rate following a large earthquake (Tohoku-Oki). Basically, if the stress decreases by logarithm of time, rapid decay of aftershocks ( $p > 1$ ) is expected.

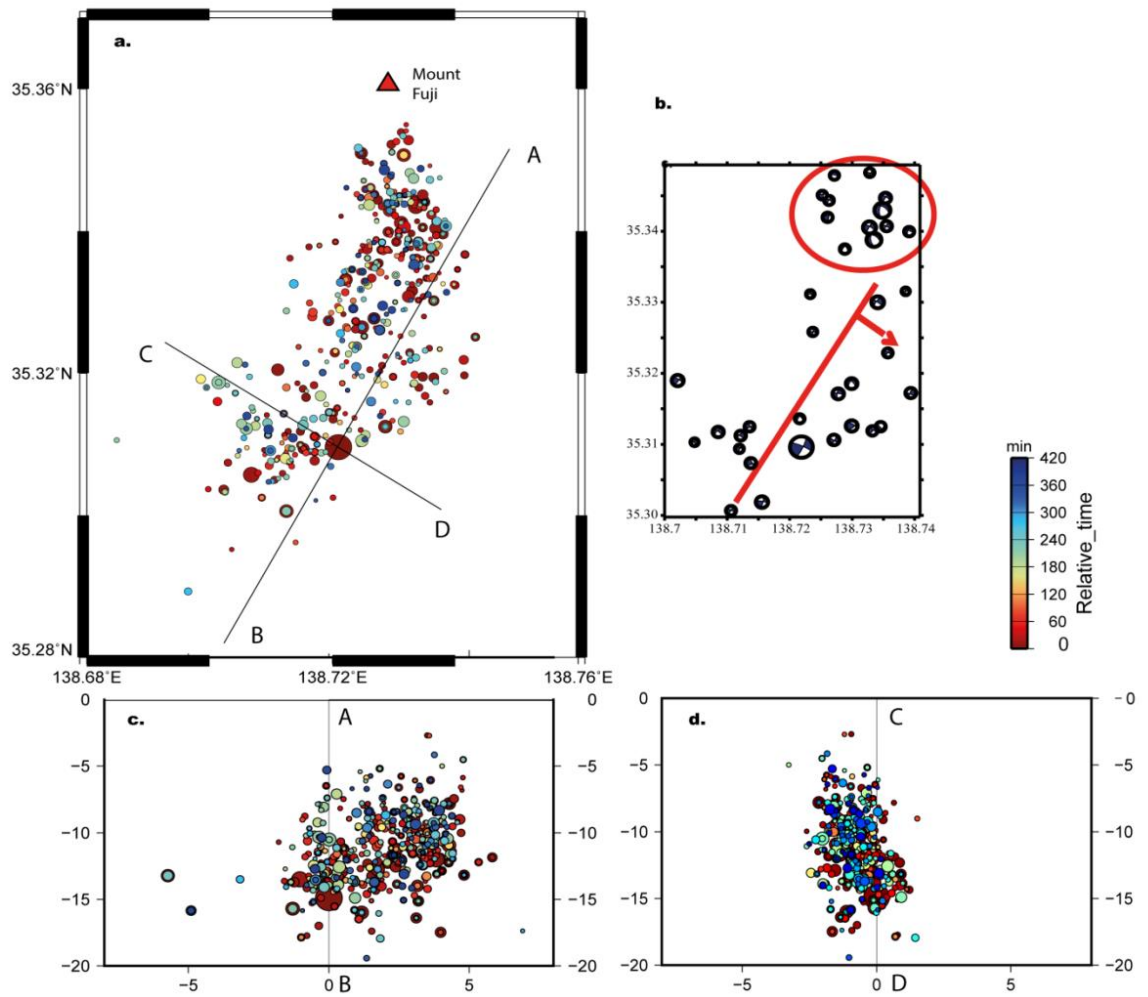


**Figure 11: Spatiotemporal distribution of MFT detections and focal mechanism.**

a) Aftershocks distribution as a function of time and magnitude. The red circles represent the early aftershocks, while the blue indicates the later earthquakes. The circles are proportional with the magnitude. b) Focal mechanism from F-net catalogue (P polarity;  $M > 2.0$ ) and fault line (red). c) – d) Aftershock distribution on the fault-plane AB parallel cross section, respectively CD perpendicular cross section .

The early aftershocks show this fast decay, which may indicate fast stressing-rate changes in the area. Klein et al. (2006) found that high  $p$  values are indicators of high temperature and accelerated stress relaxation, where the stress steps from main shocks decay faster than in the cooler rocks on the volcano flanks of Mount Fuji.

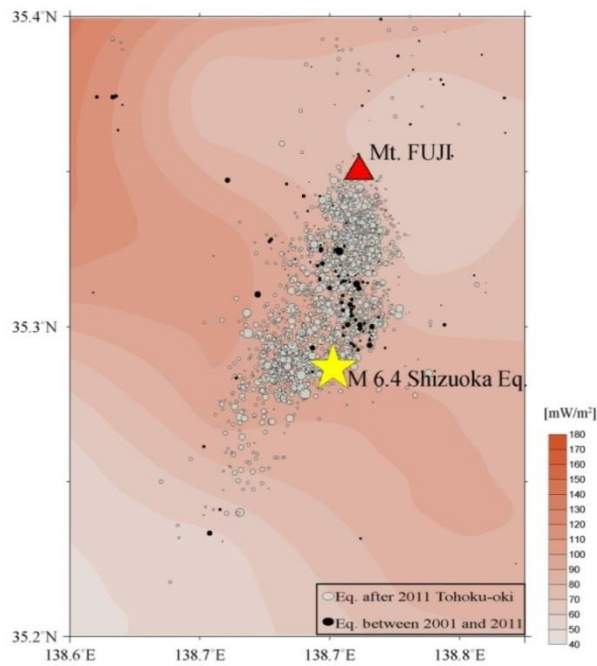


**Figure 12. Heat flow map around Mt. Fuji.** The seismicity is shown by grey circles for aftershocks and black circles for background seismicity, while the main event is represented by the yellow star. Higher heat-flow values are observed around the aftershock region.

Considering the triggering mechanism for the Shizuoka earthquake, two models have been proposed from previous studies. Fujita et al (2011) discussed the possibility of Mount Fuji erupting due to stress change caused to the magma system. The value estimated around the volcanic chamber for the static stress change caused by the Tohoku earthquake was on the order of 0.01– 0.1 bars. This value is below the threshold

to break new faults, but could trigger some perturbation in unstable faults or in the hydrothermal and magmatic systems.

Under the static triggering hypothesis, both Toda et al. (2011) and Enescu et al. (2012) calculated the static Coulomb failure stress change for the Shizuoka fault plane. The value for the stress change estimated was 0.3- 0.5 bars on the fault plane, value above the threshold for inducing changes in the seismicity rate. Thus, that static stress transfer could be a mechanism of seismic activation in Shizuoka region and the M6.4 Shizuoka earthquake is a delayed aftershock of the 2011 M9.0 Tohoku-oki earthquake.

However, Aizawa et al.,(2016) proposes a different mechanism for triggering. After performing a joint three-dimensional resistivity and isotopic analysis of the groundwater system surrounding Mount Fuji, he observed that the earthquakes were triggered within a fractured zone through which magmatic gases preferentially migrated. After modelling the fluid migration, they suggest that upwelling of fluids promoted by seismic-wave-induced shaking, caused by the arrival of surface waves from Tohoku-oki, can result in a gradual increase in pore pressure which can promote failure. Thus, their model proposes the dynamic triggering mechanism. Nevertheless, the new findings based on seismicity observations and early aftershock occurrence cannot support this triggering model.

## 2.4 Conclusions

The 2011 M6.4 Shizuoka main event occurred with a 4 days delay after the Tohoku-oki earthquake, above the magma chamber of Mountain Fuji. By closely investigating the 4 days seismicity gap from the JMA catalogue, both with a waveform-based method (MFT) and with manual inspection for some key time intervals, I could not find any evidence of locally triggered events associated with the arrival of surface waves. Based on MFT detections I model the spatiotemporal distribution of early aftershocks and I did not observe any migration of the sequence that can be associated with fluid movement. Thus, our observations on seismicity do not bring any support for the dynamic triggering and fluid migration model proposed in previous studies.

Nevertheless, it is very difficult to uniquely determine the triggering mechanism, especially in an area where the influence of both static and dynamic stress is comparable. It is possible that multiple mechanisms jointly contribute to this remote earthquake generation. The value estimated for static Coulomb failure stress change in the area is above the threshold reported for earthquake triggering, suggesting that static stress transfer can be the mechanism of seismic activation in Shizuoka region and the M6.4 Shizuoka EQ is a delayed aftershock of the 2011 M9.0 Tohoku-oki EQ.

The aftershocks are further triggered by the occurrence of the 6.4 magnitude Shizuoka mainshock. By applying the Modified Omori Law formula for the aftershocks, I noticed an increase in  $p$ -value which reflects a fast decay of the sequence, associated with quick stress relaxation and higher heat-flow values, as reported in other cases around volcanic regions.

## **.Chapter 3**

### **Remote triggering in Southwest Japan**

#### **3.1 Introduction**

The passage of surface waves generated by large earthquakes is known to cause dynamic triggering of seismicity over large distances from the source region. Since more than two decades ago, many cases of such a phenomenon were reported worldwide (e.g., Hill et al., 1993; Brodsky et al., 2000; see Hill and Prejean, 2015, for a recent review). However, in Japan, remote activation was relatively unreported (Harrington and Brodsky, 2006), although increased seismicity associated with volcanism and active faulting is observed.

Since 2011, following the occurrence of the Tohoku-oki earthquake, widespread dynamic triggering was reported (e.g., Miyazawa, 2011; Yukutake et al., 2011). Also after the 2016 Kumamoto earthquake (e.g., Enescu et al., 2016; Miyazawa, 2016), seismicity activation was observed especially at volcanoes, but also associated with active faulting environments.

However, the physical mechanisms responsible for the dynamic triggering of seismicity in different tectonic settings, two main types of models have been proposed for explaining the remote triggering by dynamic stresses (Hill and Prejean, 2015): (1) direct triggering due to frictional failure and (2) triggering by excitation of fluids in the crust.

As reported in other studies fluids may act as triggering agents in volcanic and geothermal areas (e.g., Aiken and Peng, 2014); this could explain the widespread and more vigorous activation in such regions.

In 2011, Miyazawa identified a dynamically earthquake triggering front, which propagated at similar speed as the Rayleigh waves (10 – 20 seconds period). This seismic front was observed as far as southern Kyushu, at the Ikeda volcanic area, at more than 1300 km from Tohoku-oki epicentre. The dynamic triggering seismicity around Hakone volcano, due to the surface waves from the 2011 Tohoku-oki earthquake was analysed in detail by Yukutake et al. (2011, 2013). By using a broad local seismic network, he revealed the initiation of the triggering process. The most plausible mechanism described by Yukutake et al. (2013) is likely dynamic triggering. Nevertheless, static stress changes could have played an important role (Yukutake et al., 2011, 2013; Enescu et al., 2012).

Other significant observations on dynamic triggering were made by Kato et al. (2013), who analysed the Hida region. He discussed the triggering by both dynamic and static stress changes in the region. Similarly, Shimojo et al. (2014) investigated the seismicity increases instantly after the megathrust event, in Northern Nagano region. His findings indicate that the activation was initiated dynamically and intensified due to excitation of crustal fluids from this geothermal region.

In the mentioned studies, aseismic transients (slow-slip or fluid movements) could be responsible for the triggering process. In volcanic and geothermal regions, the triggered sequences indicate migration and swarm-like characteristics, that are a clear signature of aseismic transients (e.g., Kumazawa and Ogata, 2013; Shimojo et al., 2014; Kosuga, 2014).

### 3.2 Method and Data

For analysing the seismic activation in Southwest Japan, I used the earthquake catalogue data provided by the Japan Meteorological Agency (JMA) and the high-sensitivity Hi-net, respectively the broadband F-net waveform data from the National Research Institute of Earth Science and Disaster Resilience (NIED).

At first I created a catalogue of earthquakes occurring in Southwest Japan for the first 30 minutes after the 2011 megathrust earthquake, which I used throughout my study. All the earthquakes that I detected and locate using the high-frequency seismograms are shown in Table 1. By using the HYPOMH program developed by Hirata and Matsu'ura,(1987) and the 1D velocity model provided by the JMA, I localized the remotely triggered earthquakes, which are plotted in . Figure 1, alongside the background seismic activity, retrieved from the JMA catalogue.

The locally triggered events were identified using a two-way Butterworth Bandpass filter in the 10-30 Hz frequency range. It was observed in previous studies, (e.g., Shimojo et al. 2014, Enescu et al. 2016), that such a filtering method ensures a good detection of remotely triggered events, by avoiding the high-frequency noise. For most of the cases, I was able to localize the remote triggered events by identifying the *P*- and *S*-wave arrival times.

It is important to mention that the identified triggered events are not from the JMA catalogue data. Due to the impressive number of aftershocks and the large amplitude surface waves that might obscured many small events, the JMA catalogue is incomplete for a short interval after the megathrust occurrence. The migration of the earthquake front propagating in Southwest Japan was addressed by Miyazawa (2011).

The triggered areas he identifies are similar with the ones from this study. However, I focus on the type and characteristics of surface waves observed at the triggering sites, a topic that has not been addressed previously.

Number	Hour	Minute	Second	Latitude	Longitude	Depth (km)	Magnitude	Area
1	14	51	51.09	34.804	137.173	38.49	3.0	Aichi
2	14	53	26.73	35.040	137.194	40.97	3.1	Aichi
3	14	55	5.17	34.981	137.182	27.67	2.9	Aichi
4	14	51	0.64	35.741	134.981	13.99	2.6	Hyogo
5	14	52	26.51	35.683	134.751	13.54	2.3	Hyogo
6	14	55	29.45	35.736	134.982	13.52	2.5	Hyogo
7	14	51	38.21	33.873	134.474	31.43	3.1	Tokushima
8	14	54	55.40	33.890	134.532	33.78	1.8	Tokushima
9	14	55	11.41	34.011	134.531	35.16	2.0	Tokushima
10	14	55	30.30	33.734	134.547	36.86	2.2	Tokushima
11	14	52	36.39	33.123	131.233	8.20	2.7	Kyushu
12	14	53	28.90	31.234	130.573	1.62	2.4	Kyushu
13	14	54	26.89	33.113	131.203	7.10	2.6	Kyushu
14	14	56	33.17	33.107	131.208	9.76	1.7	Kyushu
15	14	57	20.27	33.702	130.226	8.57	2.4	Kyushu
16	14	58	6.63	33.106	131.185	4.50	1.3	Kyushu
17	14	59	11.21	32.756	130.068	0.38	1.2	Kyushu
18	14	59	51.69	33.298	131.435	1.51	1.1	Kyushu
19	15	1	24.82	33.269	131.402	3.79	0.9	Kyushu
20	15	3	27.19	32.949	130.993	1.32	0.8	Kyushu
21	15	5	5.23	33.302	131.429	1.60	0.8	Kyushu
22	15	5	32.63	33.298	131.441	1.49	0.8	Kyushu
23	15	13	42.08	32.891	130.950	8.71	1.9	Kyushu
24	15	13	42.95	32.924	131.004	16.61	1.8	Kyushu
25	15	14	18.14	32.979	131.052	22.18	1.4	Kyushu
26	15	14	20.75	33.297	131.434	1.48	1.2	Kyushu
27	15	14	31.10	32.893	130.949	9.67	2.5	Kyushu

Number	Hour	Minute	Second	Latitude	Longitude	Depth (km)	Magnitude	Area
28	15	14	32.82	32.926	131.006	22.24	2.3	Kyushu
30	15	15	11.96	32.892	130.951	9.25	2.5	Kyushu
31	15	16	28.06	33.293	131.492	0.95	0.9	Kyushu
32	15	17	3.55	32.865	130.970	10.86	2.0	Kyushu
33	15	17	6.63	33.034	131.111	20.95	1.8	Kyushu
34	15	17	27.08	32.898	130.947	9.29	0.6	Kyushu
35	15	17	44.51	32.886	130.938	6.79	0.5	Kyushu
36	15	19	12.22	33.385	131.188	15.20	1.9	Kyushu
37	14	55	32.34	35.496	133.843	24.45	2.7	Tottori

**Table 1. The catalogue of early triggered events in Southwest Japan, following the 2011 M9.0 Tohoku-oki earthquake.** The earthquakes were detected in the areas shown in Figure 1, after the occurrence time of the Tohoku-oki megathrust (March 11, 2011; 14:46:18). The table is listing their origin time (hour, minute second), location (latitude, longitude and depth), magnitude and geographic area.

Next, I used low-frequency F-net and Hi-net waveform data, which was processed in the frequency domain of 0.01-0.2 Hz, following Maeda et al. (2011) approach. By applying a specifically designed recursive filtering, the Hi-net waveform data can be used to retrieve long-period ground motions.

I observed the correlation between remotely triggered local events, shown at each station on the vertical component of the velocity seismograms (filtered in the 10-30 Hz range), and the arrival of surface waves from the Tohoku-oki earthquake, shown on the vertical, radial and transversal displacements seismograms (filtered in the 0.01 -0.1 Hz range).

### 3.3 Dynamic triggering observed in Southwest Japan

#### 3.3.1 Seismicity activation following the 2011 $M_w$ 9.0 Tohoku-oki earthquake

After the occurrence of the 2011  $M_w$ 9.0 Tohoku-oki earthquake, a front of remote triggered earthquakes propagating along Southwest Japan was reported in correlation with surface waves arrival. Nevertheless, the characteristics of the dynamic seismic activation can be investigated in more detail.

Based on the prefecture name where I identify the locally triggered events, the areas investigated in this study are Aichi, Tokushima, Hyogo, Tottori, Fukuoka, Nagasaki, Oita and Kagoshima. Note that the area labelled “Oita” includes the Aso and Yufuin-Beppu volcanic sub-areas (discussed in Chapter 4).

I did not included in the investigation the activation of seismicity observed at Hida Mountain (Kato et al., 2013) and the one around Izu Peninsula (Toda et al., 2011; Enescu et al., 2012), including Hakone volcano area (Yukutake et al., 2011, 2013). All these cases were analysed in details before; both dynamic and static stress changes from Tohoku-oki earthquake played a triggering role.

In Figure 1 I indicate the remotely activated areas: Aichi and Tokushima, (depths around 30 – 45 km), Hyogo and Tottori, (depths around 15 – 25 km) and Fukuoka, Nagasaki, Oita and Kagoshima in Kyushu Island a (relatively shallow depth of 0 – 15 km).

The remotely triggered earthquakes in regions Aichi and Tokushima occur close to the subduction interface of the Philippine Sea Plate under the Japanese Islands, (e.g., Hirose et al., 2008). The events detected in Hyogo, Tottori and Fukuoka areas are

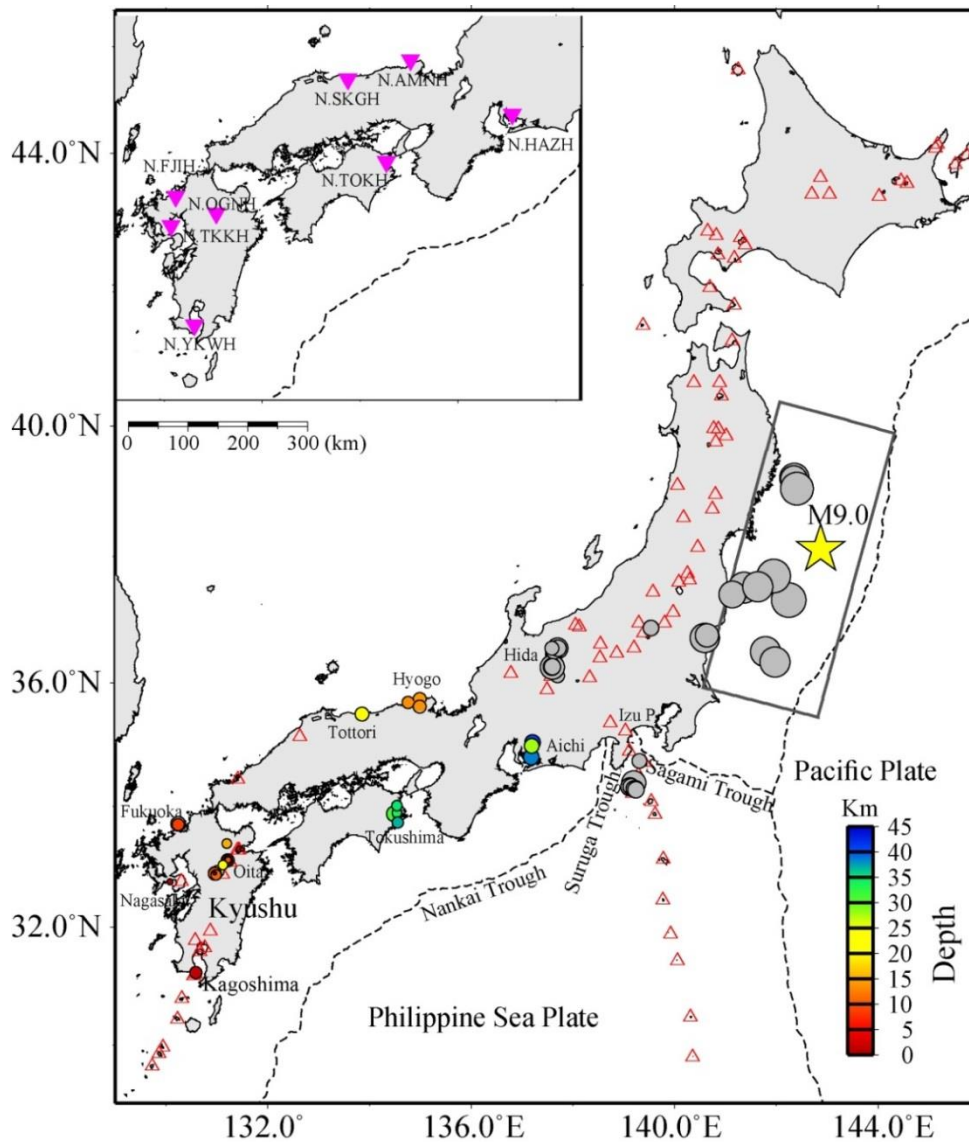


**Figure 1. Distribution of the seismic activity in Japan for the first 30 minutes after the 2011  $M_w$  9.0 Tohoku-oki earthquake (2011/03/11 14:46:18.12 JST).** The Tohoku-oki mainshock is shown by yellow star, JMA-catalogue events are shown by grey circles, while coloured circles represent manually detected epicentres (Table 1), coloured as a function of depth. Volcanos are plotted as red triangles. The inset shows the NIED Hi-net stations (inverted purple triangles) used in Figure 2.

associated with a strike-slip environment (e.g., Terakawa and Matsu'ura, 2010; Toda and Enescu, 2011), while the events from Oita, Nagasaki and Kagoshima occur in geothermal/volcanic areas, that are known as extensional tectonic regions.

Since these areas are located at relatively large distances from the Tohoku-oki earthquake (Figure 1), the initiation of seismicity activation by static stress changes from the megathrust event unlikely (Toda et al., 2011; Miyazawa, 2011).

Nevertheless, I verified this assumption by using the model of Suzuki et al. (2011) as source for the Tohoku-oki rupture model and nodal planes of F-net (NIED) CMT focal mechanisms considered representative for the local faulting structures. I selected earthquakes with magnitude above 3.0 (from 1997 to 2017) in the areas mentioned above, as receivers and calculated the Coulomb static stress changes.

Using an apparent coefficient of friction  $\mu' = 0.4$  (variations within 0.2 – 0.8 produced equivalent results), the estimated stresses were on the order of 0.01 MPa. According to Stein (1999), the value of 0.01 MPa is an effective stress triggering threshold for seismic events. For example, the largest dynamic stress calculated by Miyazawa (2011) in Kyushu, where I observed the most significant activation (see Chapter 4) was at least one order of magnitude larger than the values obtained for static stress, which were less than 1 kPa. Thus, it is reasonable to say that the role of static stress transfer from the megathrust in triggering seismicity in the investigated areas was not significant.

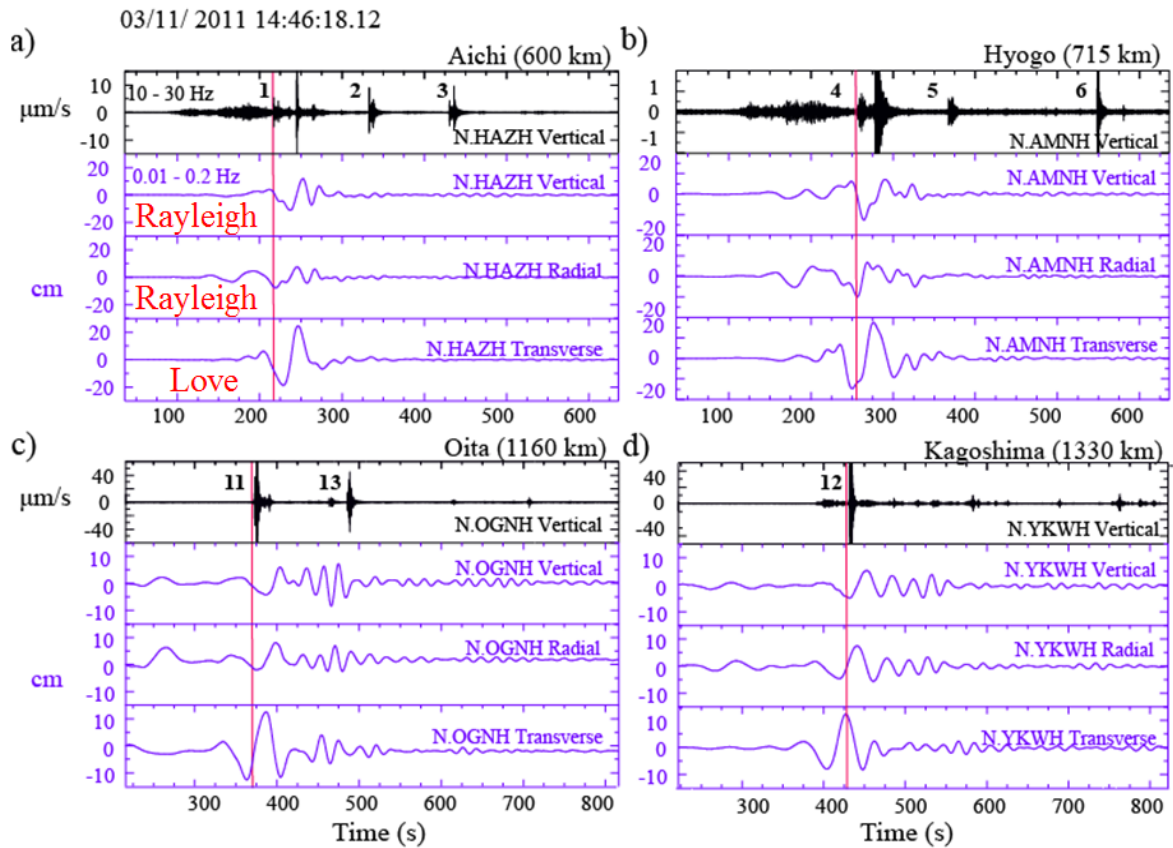


**Figure 2. Correlation between the remote earthquake triggering in Southwest Japan and the arrival of surface waves from Tohoku-oki mainshock.** The high-frequency (10–30 Hz) vertical velocity seismograms from Hi-net stations (NIED) are shown in black, while the low-frequency (0.01 – 0.1 Hz) vertical, radial and transverse displacement components seismograms are shown in blue. Time (s) represents the number of seconds relative to the Tohoku-oki mainshock; a) Triggering in Aichi area, shown at HAZH station; b) triggering in Hyogo area, at AMNH station; c) Oita area (more precisely, close to Kuju and Aso volcanoes), at the OGNH station; d) Kagoshima area, shown at YKWH station; The numbers indicate manually detected events (listed in Table 1).

In Figure 2, I show the characteristics of immediate triggering for four of the triggered regions: Aichi, Hyogo, Oita and Kagoshima. The high-frequency vertical component (filtered in the 10 – 30 Hz range) velocity seismograms shows locally triggered events, while the low-frequency (filtered 5 – 100 s) displacements seismogram for the vertical, radial and transverse components, show the arrival of surface waves from Tohoku-oki mainshock. Both Love and Rayleigh wave trains correlate with the first events triggered in each of those regions (see Table 1).

The Love wave displacement amplitudes seen on the transverse components have significantly larger amplitudes than the Rayleigh waves seen on the vertical and radial components. Moreover, the triggering in Hyogo, Oita and Kagoshima areas from Figure 2b, c and d, occurred close or at the peak of Love wave arrival (same was observed in Tokushima region).

For example, the displacements amplitudes for Love waves recorded at YKWH station in Kagoshima, shown in Figure 2d, are of 12.4 cm, while for the Rayleigh waves, the amplitude is significantly smaller (5.4 cm, seen on the vertical component of the displacement seismogram). To be precise in performing the correlation, both the low-frequency and high-frequency waveforms were time corrected, considering the location and occurrence time of the first triggered event in each region. Note that the average considered phase velocities for P-wave, Love and Rayleigh waves are 6.5 km/s, 4.1 km/s and 3.9 km/s, respectively. Small variations of these values do not influence significantly the results (since the triggered events occurred close to the corresponding Hi-net station).

Volcanic regions where fluids are active agents, like the remotely activated areas from Kyushu Island, are expected to respond to Rayleigh-wave due to excitation by compressional motions. However, the observations seem to indicate that Love waves have initiated the triggering. In the other regions where active faults are involved, the initiation due to shearing motion by the Love waves was not a surprising result.

Considering the source-receiver geometry and the amplitude of shaking, it is challenging to estimate the dynamic stresses at each triggering site (Gonzalez-Huizar and Velasco, 2011), due to the fact that the earthquakes remotely triggered by the Tohoku-oki earthquake are small and their focal mechanism can't be determined. By using the focal mechanisms from past events as receiver source to calculate dynamic stress changes might provide biased results due to the observation that the focal mechanisms of the triggered events by the megathrust earthquake can be sometimes 'atypical' (e.g., Toda et al., 2011).

In Kyushu Island I observed that the dynamic triggering occurs during the passage of surface waves with relatively large periods (20 to 50 seconds). I show in Figure 3a the amplitude spectra at Ibusuki geothermal area, close to YKWH station. Usually, surface waves of 10 s to 25 seconds period are reported as being efficient at dynamically triggering earthquakes (e.g., Brodsky and Prejean, 2005; Enescu et al., 2016).

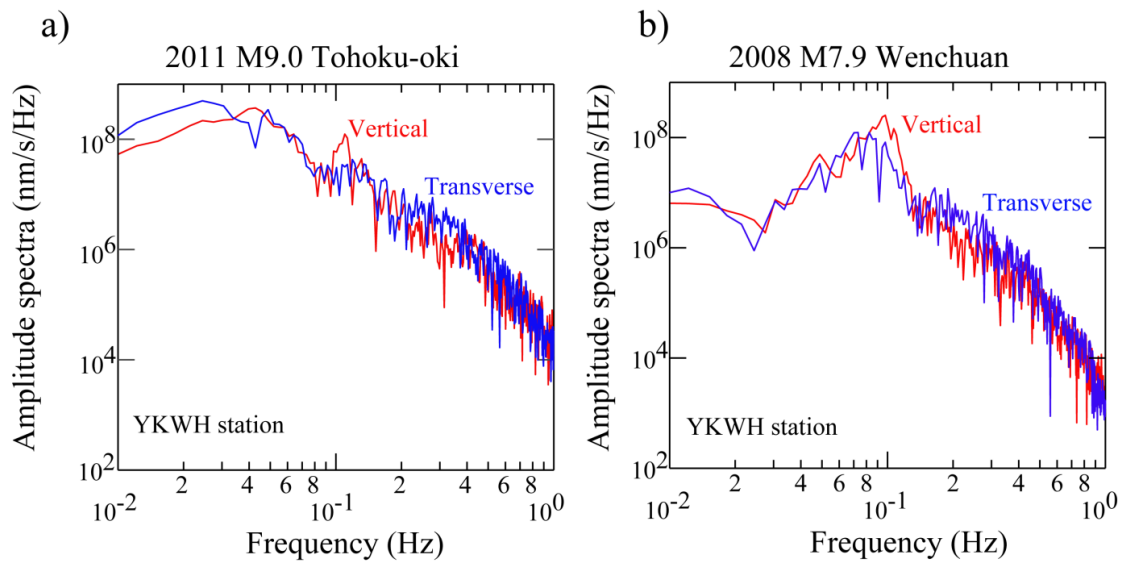


**Figure 3. Amplitude spectra of surface waves in Kagoshima, at station YKWH.** Amplitude spectra (nm/s/Hz) versus frequency (Hz), using the filtered velocity seismograms (0.01-1 Hz) for the vertical (red) and transversal (blue) components. a) for the 200-s surface wave train (see Figure 2d) of the 2011 Tohoku-oki earthquake; b) for the 200-s surface wave train (see Figure 5c) after the 2008 Wenchuan earthquake.

### 3.3.2 Evidence of triggering potential in Kyushu by both surface waves from the 2008 $M_w$ 7.9 Wenchuan earthquake

I showed in the previous section the possibility of large-amplitude Love waves to cause the initiation of triggering locally events following the Tohoku-oki earthquake. Due to the close arrival between the two surface waves, I will further investigate the triggering potential of both Love and Rayleigh waves by searching remote activation that might occur after teleseismic large events.

After performing a systematic analysis for remote triggering observed in Japan, Harrington and Brodsky (2006) found evidence of remote triggering following only the 2004 M9.0 Sumatra earthquake , . The activated area in the Kyushu Island is similar to the area labelled “Kagoshima” in this study).

Next, I searched in the ANSS catalogue for events with magnitude  $M \geq 7.5$  which occurred after 2005. Considering the amplitude of shaking recorded at Hi-net stations, close to volcanic sites in Kyushu, I classified the events from Table 2. The largest surface wave amplitudes that correspond to dynamic stresses above a few kPa have been observed after the 2008 M7.9 Wenchuan, 2012 M8.6 Sumatra, 2005 M8.6 Nias, 2007 M8.1 Solomon Islands, and 2007 M8.4 Sumatra earthquakes.

Event name	Date	Origin time (JST)	Latitude	Longitude	Depth	Magnitude
Nias	29/03/2005	01:09	2.05	97.06	33.7	8.6
Solomon Island	02/04/2007	05:39	-8.43	157.06	10.0	8.1
Sumatra Islands	12/09/2007	20:10	-4.44	101.37	34.0	8.5
Wenchuan	12/05/2008	15:28	31.02	103.37	19.0	7.9
Sumatra Islands	11/04/2012	17:38	2.31	93.06	20.0	8.6

**Table 2. Teleseismic events from the ANSS catalogue.** Investigated earthquakes with magnitude  $M \geq 7.5$ , which occurred after 2005 and that could generate remote triggering in Southwest Japan.

Although small events were observed in Kagoshima area after the 2012 Sumatra earthquake, it was difficult to separate from the background noise. Nevertheless, following the 2008 Wenchuan earthquake, a more clear triggering was observed during the passage of surface waves. The rest of teleseisms from Table 2 were non-triggering events.

I will further investigate the locally triggered earthquakes by the Wenchuan earthquake at Oita and Kagoshima areas (Figure 4) ,using the same method described previously. Although at some stations *P*- and *S*-wave arrivals were recognizable, the number of available phases was not sufficient for locating these events (Figure 5).

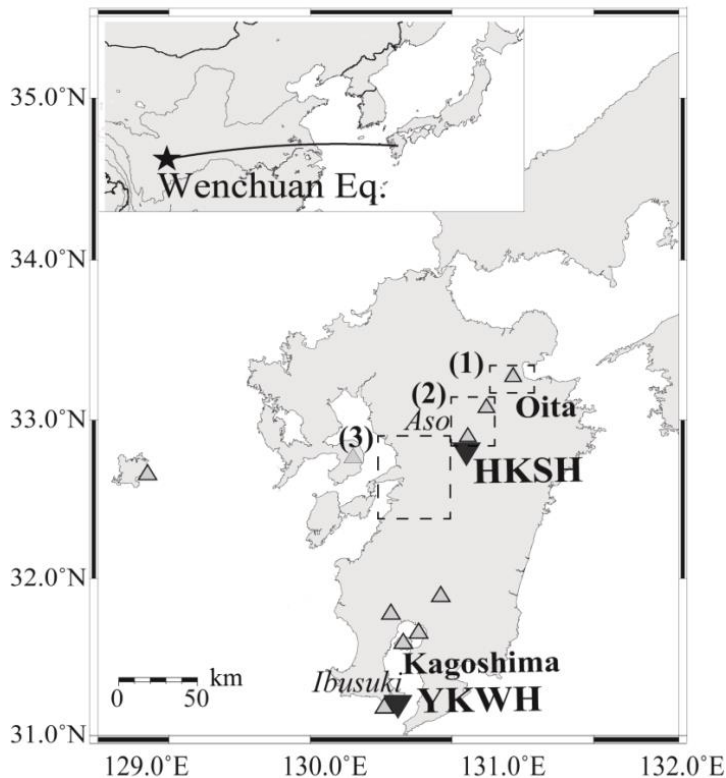


**Figure 4. Remotely triggered areas in Kyushu by the 2008/5/12 15:28:01 (JST)  $M_w$ 7.9 Wenchuan earthquake.** Volcanoes in Kyushu (grey triangles) and NIED Hi-net stations (black inverted triangles) used in Figure 6; Dashed rectangles represent the area labelled “Oita”, with two distinct volcanic sub-areas, (1) Yufuin-Beppu and (2) Aso, respectively area (3) the 2016 Kumamoto rupture area; the inset shows a regional map with the location of the 2008 Wenchuan earthquake and the travel path of the surface waves.

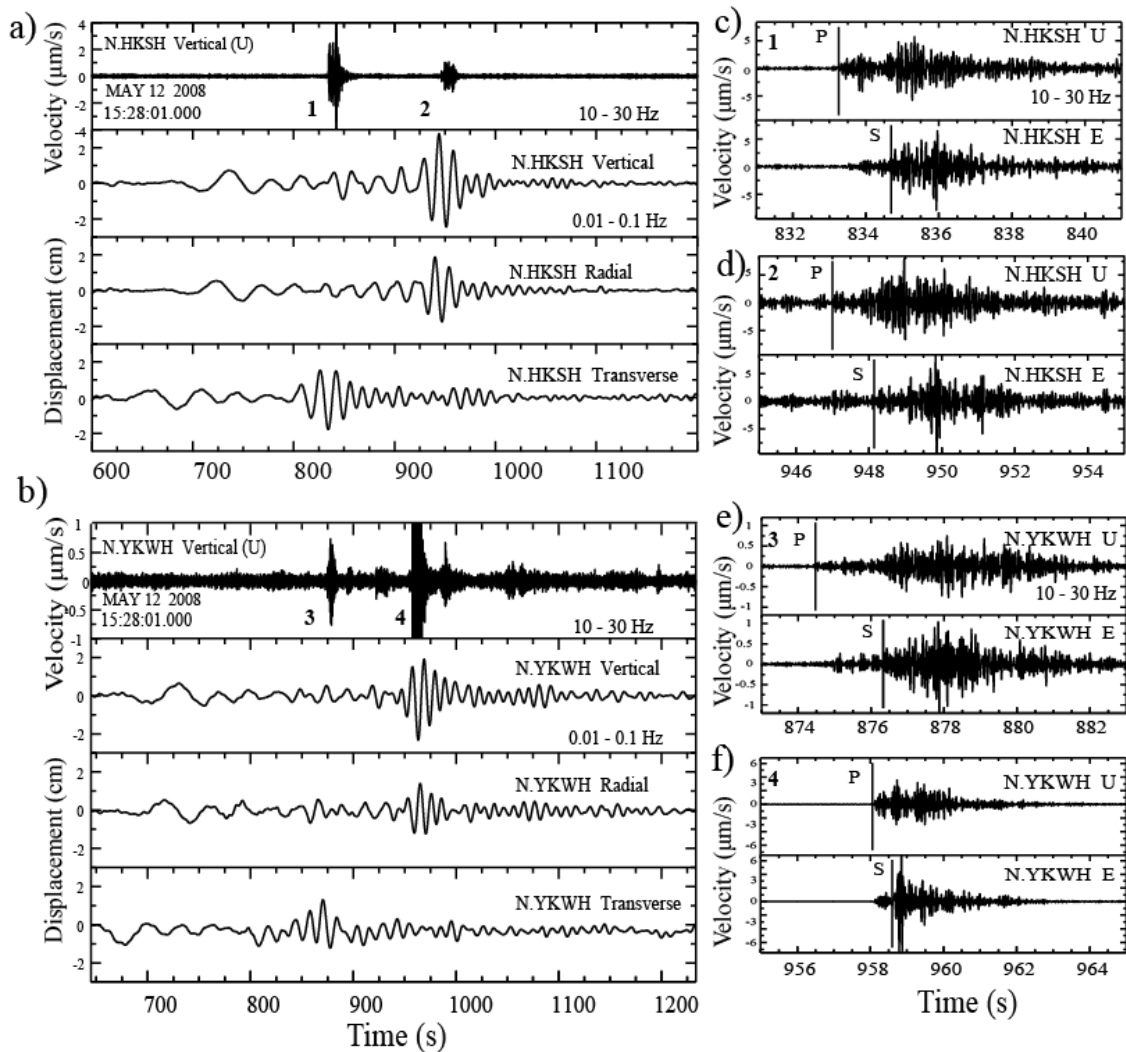


**Figure 5. Correlation between the remote triggering in Kyushu and the arrival of surface waves from the 2008 Wenchuan earthquake.** a) Triggered events shown on the high-frequency (10–30 Hz) vertical velocity seismogram at HKSH station (close to Aso volcano), followed by the low-frequency (0.01 – 0.1 Hz) vertical, radial and transverse displacement seismograms, respectively, relative to the origin time of the Wenchuan earthquake (seconds). b) Same as in (a), but at YKWH station (in southern Kyushu); c-f) Plots showing the P- and S-wave arrivals on vertical (U) and horizontal (E-W) velocity seismograms, respectively, for the local events that are likely triggered by the passage of Love ((c), (e)) and Rayleigh ((d), (f)) waves from the Wenchuan earthquake.

In Figure 5a and 5b, the correlation between the distinct arrival of Love and Rayleigh waves and the locally triggered events can be seen. Around Aso volcano from Oita area and in Kagoshima area the triggering coincides with surface waves arrivals with periods of 10 to 20 seconds (Figure 3b), similar with other documented cases (e.g., Hill and Prejean, 2015; Enescu et al., 2016).

Thus, a possible dynamic triggering scenario can be proposed for remote triggering observed in Kyushu. Triggering is initiated by the arrival of Love wave trains on fault segments well-lubricated by the presence of fluids at or close to volcanic areas. The faults that are brought at or close to failure are further activated by Rayleigh wave trains, which can cause fluid excitation, inducing additional cracking. In the Nankai Through a similar scenario for triggering was proposed (Chao et al., 2012), based on observations of both surface waves triggering of tectonic tremor following the 2011 Tohoku-oki earthquake.

After investigating other remote teleseismic events that occurred after 2005, as well as the 2008 Wenchuan earthquake, I did not find other evidence for triggering at non-volcanic sites. The dynamic stresses generated by the Wenchuan earthquake were in the 30 – 80 kPa range (for non-volcanic sites), while teleseismic events produced much lower values, in the 10 – 40 kPa range for the 2012 Sumatra earthquake and on the order of 10 kPa or less for the 2005 Nias, 2007 Sumatra and 2007 Solomon Islands earthquakes. Moreover, the seismic activation observed at the volcanic sites in Kyushu after the Wenchuan earthquake was relatively weak. It is possible that this activation occurs only during the passage of surface waves from the mainshock, if the area is not close to failure.

### 3.4. Conclusions

The seismicity activation in Southwest Japan was initiated due to the strong shaking caused by the passage of both Love and Rayleigh waves from the 2011 Tohoku-oki earthquake. The first events in each of the triggered areas occurred during the passage of large surface waves from the mainshock.

Although this result is expected, after estimating the dynamic stress change values, following Peng et al. (2009) approach, it is possible that the strong shaking by the passage of Love waves initiated the triggering process. In Kagoshima, at station YKWH, on the transverse component, which is useful for observing the Love wave trains arrival, the estimated value of 0.13 MPa (about 10 times above the triggering threshold) is capable of triggering seismicity. The displacements on transverse components indicate that Love waves played a significant role in initiating remotely the seismicity activation, after the megathrust event.

We have also noticed that the surface waves responsible for the dynamic triggering after the 2011 Tohoku-oki earthquake are characterized by relatively high periods (20 – 50 s) compared to those (10 – 25 s) usually reported as most efficient at remotely triggering earthquakes. The large shaking (i.e., dynamic stresses) associated with these larger period surface waves was likely the dominant factor responsible for event-triggering.

By further investigating remote triggering in volcanic regions in Kyushu, around Aso volcano and Ibusuki geothermal field, the possibility that the Love waves initiated the triggering was confirmed after the occurrence of the local events detected following the distinct arrival of surface waves from the 2008 M7.9 Wenchuan earthquake. Estimated

dynamic stresses near Aso volcano estimated from the velocity seismograms at HKSH station were about 0.1 MPa, similar to the values at YKWH station, in Ibusuki.

Based on the results, the sharing motion, induced by the passage of Love waves from the remote large earthquake on well-lubricated local faults, may have facilitated and started failure in the investigated areas, while the subsequent passage of Rayleigh waves triggered also local earthquakes, especially in volcanic and geothermal regions, where fluids are involved.

The maximum values for dynamic stress from the investigated teleseismic events mentioned in the previous section, estimated at volcanic regions in Kyushu were significantly smaller than those from the 2011 Tohoku-oki and 2008 Wenchuan earthquakes.

Thus, I was able to identify remote triggering in different tectonic environments, where the activation correlates better with the arrival of Love waves, when compared with the arrival of Rayleigh waves. To confirm this observation, I investigate other teleseismic events that might have dynamically triggered seismicity in Southwest Japan. Due to the large distance, distinctive Love and Rayleigh waves arrival time was observed, especially for the 2008 M7.9 Wenchuan earthquake. I identified local events associated with both surface waves arrivals in volcanic and geothermal regions Kyushu Island. Well-lubricated local faults could start the failure process due to the sharing motion caused by these waves.

## **.Chapter 4**

### **Decay characteristics of remote seismicity in Southwest Japan**

#### **4.1 Introduction**

After the occurrence of the 2011 M9.0 Tohoku-oki earthquake, a front of remote triggered earthquakes propagating along Southwest Japan was reported in correlation with surface waves arrival. Nevertheless, the characteristics of the dynamic seismic activation can be investigated in more detail. Using unprocessed NIED waveform data, I analysed in the previous chapter the remote triggering process and the seismicity activation observed in Southwest Japan.

In this chapter, I would like to investigate in more detail the remote seismicity activation in Southwest Japan, focusing on the temporal extent and the decay characteristics of stacked and individual sequences observed in the different tectonic environments activated after the 2011 Tohoku-oki earthquake.

Also, after the 2016 Kumamoto earthquake, widespread remote triggering was observed in the Japanese Islands, small local events being dynamically triggered at distances of more than 1600 km (Hokkaido Island) by the passage of surface waves. A strong directivity effect, as well as an increased triggering potential after the 2011 Tohoku-oki earthquake could be the probable causes of such widespread activation (Enescu et al., 2016).

The  $M_w$ 7.3 mainshock was reported to trigger dynamically a large event (with magnitude  $M_w$ 5.9) in the geothermal region Yufuin-Beppu in, Kyushu (e.g., Uchide et al., 2016; Miyazawa, 2016). The same region was remotely activated by the 2011 Tohoku-oki earthquake (Miyazawa, 2011).

Since the Oita geothermal area in Kyushu was activated both after the 2011 megathrust earthquake, and also dynamically triggered following the 2016  $M$ 7.3 Kumamoto earthquake, I compare the decay of “normal” aftershocks, triggered by the static stress changes due to the Kumamoto mainshock rupture, with that of dynamically initiated seismicity at the geothermal area.

## **4.2 Method and data**

In order to investigate the short-term activation of remote seismicity at areas where dynamic triggering was confirmed previously (see Chapter 3), I combined the manually detected earthquake dataset (see Table 1) with the earthquake catalogue from JMA.

I selected from the JMA-catalogue, the earthquakes that occurred within 30 km radius from the epicentres of the manually detected events, at depths less than 50 km. If the event occurred within less than 2 s and less than 5 km from the manually detected earthquake, I considered the two events identical; only the manually detected event was selected in the new catalogue. Similar results were obtained for variation of the radius in the 20 to 40 km range. Next, I show in map view (Figure 1) the results of the selection, considering a time window of 120 days, centred on the occurrence of the 2011 Tohoku-oki earthquake.

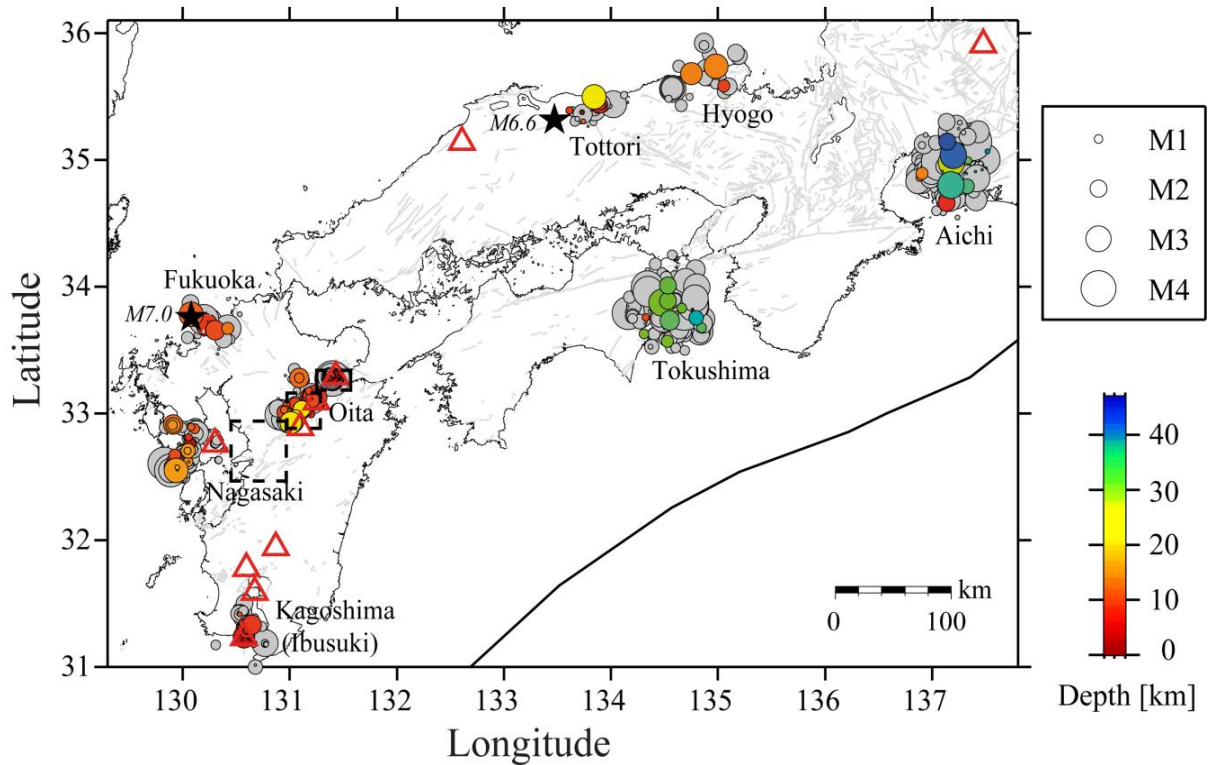


**Figure 1. Areas in Southwest Japan with observed dynamic triggering by the 2011 Tohoku-oki earthquake.** Grey circles represent earthquakes from the JMA catalogue, selected for a radius of 30 km around the first manually detected events after the Tohoku-oki mainshock, for each of the triggered regions, for a time interval of 60 days before and after the March 11, 2011. The coloured circles show the seismic activity (JMA catalogue and manual detections) during the first week after the mainshock. Black stars show the epicentres of the 2005 M7.0 Fukuoka earthquake and the 2016 M6.6 Tottori earthquake, respectively. Dashed rectangles mark the same areas as in Figure 6. Red triangles represent volcanoes.

For the improved catalogue data, I determined the magnitude of completeness ( $M_c$ ), by using the Entire Magnitude Range method (EMR) (Woessner and Wiemer, 2005). Next, I estimate the  $b$ -values (of the frequency-magnitude distribution) and the  $p$ -value from the Modified-Omori Law, for  $M \geq M_c$ . The  $b$ -value was determined using the Maximum Likelihood approach (MLM) (Aki, 1965).

The parameters of the Modified Omori law,  $n(t) = K/(t + c)^p$  - where  $n(t)$  is the frequency of aftershocks per unit time, at the time  $t$  from the mainshock and  $p$ ,  $c$ , and  $K$  are constants - are determined by maximizing the logarithm of the likelihood function (Ogata, 1983). Standard errors of parameters are obtained from the inverse of the Hessian matrix of the likelihood function (Ogata, 1983).

#### **4.3 Short-term activation following the 2011 Mw 9.0 Tohoku-oki earthquake**

For the short-term activation following the Tohoku-oki earthquake, I plot in Figure 2, time versus cumulative number of events for the epicentres shown in Figure 1, in order to detect the temporal extent of remote activation. This plot represents the stacking of seismicity in the remotely triggered regions identified in the previous chapter. Stacking is a usually used to enhance the “useful” but weak signal from the “background” activity (e.g., Enescu et al., 2009), especially when discussing properties of aftershocks or foreshocks that occurred in a region where the sequence does not indicate a strong activity (small number of events).

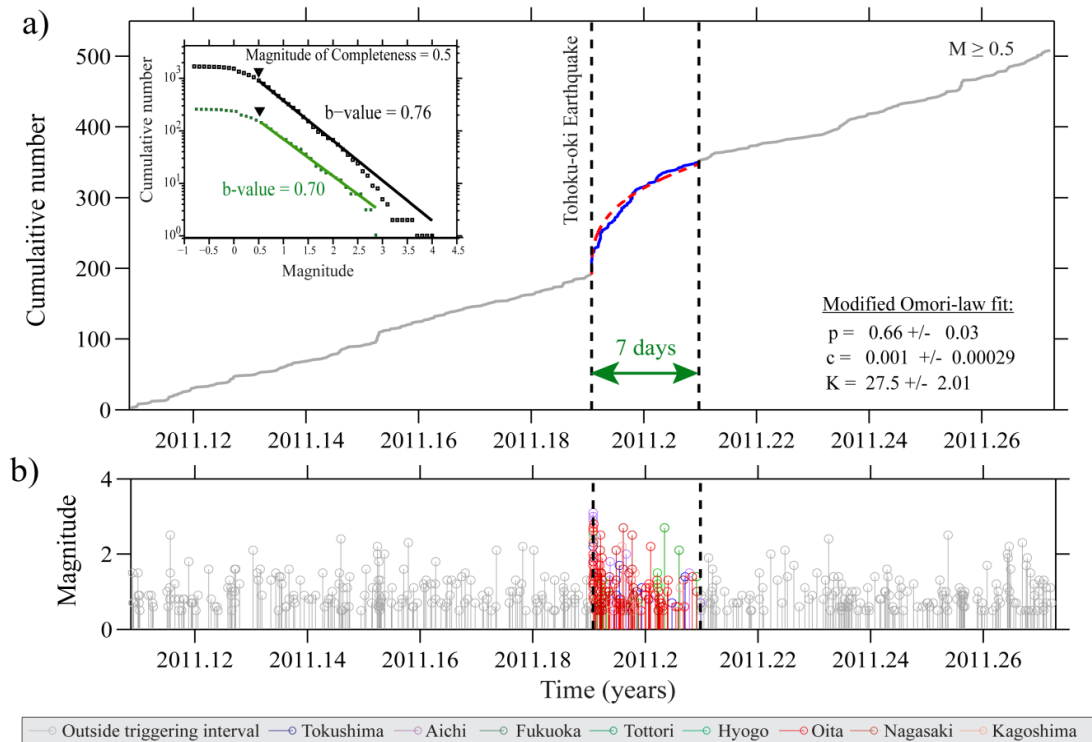


**Figure 2. Temporal evolution of seismicity before, during and after the remote triggering activation.** a) Cumulative number of triggered events versus time, in the selected areas (Figure 1). The curve during the 7-day period after Tohoku-oki mainshock is plotted in blue; grey is used for the other time periods. The red dotted curve represents the modified Omori-law fit, with parameters:  $p = 0.66 \pm 0.03$ ,  $c = 0.001 \pm 0.00029$ ,  $K = 27.5 \pm 2.01$  (see text for details). The left inset shows the frequency-magnitude distribution of events during the whole observation period (shown in black;  $b$ -value =  $0.76 \pm 0.02$ ,  $a$ -value = 3.34), respectively the 7 days interval (shown in green;  $b$ -value =  $0.70 \pm 0.05$ ,  $a$ -value = 2.48), calculated for  $M \geq M_c = 0.5$ , as determined by the EMR method. Note that the same  $M_c$  is obtained for the activated seismicity during the 7-days interval discussed in the text. b) Magnitude versus time distribution for the same time-period as in (a); colours show events occurred for the 7-may triggering period, in various triggered areas (see legend), while grey is used for other time periods.

The cumulative number of earthquakes (with magnitudes larger than the overall completeness magnitude,  $M \geq M_c = 0.5$  – see inset of Figure 2, upper plot and related explanations in figure’s caption) shows a clear, albeit relatively weak activation that coincides with the timing of the 2011 Tohoku-oki earthquake (Figure 2).

The background seismicity rate in the investigated regions, for events with magnitude  $M \geq 0.5$  that occurred from the beginning of 2011 until the occurrence of the megathrust event, was estimated at the rate of 5 events/day. In the first (67 events/day) and second (28 events/day) days after the Tohoku-oki, the seismicity rate increased 11.2 and 4.7 times, respectively, compared with the rate of the events in the day before the occurrence of the megathrust (6 events/day). The seismicity rate after one week from the megathrust event returned to pre-Tohoku-oki earthquake levels (6 events/day).

The 7-days relative seismicity increase observed after the 2011 Tohoku-oki earthquake in the triggered areas indicates a clear decay with time, which can be fitted by the Modified Omori law, as shown in Figure 2 (dotted red curve) .

The relatively low ( $\sim 0.66$ )  $p$ -value obtained for the fitting needs to be interpreted with caution due to the fact that the level of catalogue incompleteness can be problematic at short times after the megathrust earthquake. According to Utsu et al. (1995), the “contamination” with background seismicity could bias the parameter towards smaller values. However, I obtained equivalent results for higher magnitude thresholds ( $M = 0.7, 1.0$ ).

The return period of seismicity rates to the background level of 6 events/day, assuming the estimated Omori-law parameters (Figure 2), should last about 10 days. Such a result suggest that despite an overall slow decay of seismicity rates associated

with low  $p$ -value, the weak seismicity activation in the studied areas returns to the background level in 7 ~ 10 days.

#### **4.4 Activation at volcanic and non-volcanic regions**

By extending the analysis for the remote seismicity activation, using an improved JMA catalogue, I was able to observe that the stacked seismicity after the occurrence of the megathrust event has a significant, but weak increase, which was followed by a relatively slow decay towards the background level, in just a few days. Due to the small number of events, although I discussed in the previous section the slow decay for the stacked seismicity, each individual remotely activated area might have different characteristics

The remote triggering in “Aichi” and “Tokushima” regions occurs close to the subduction interface. While it is difficult to separate between background and activated seismicity in this environment, the instant triggering associated with arrival of surface waves was clearly observed on seismograms (see Figure 2, Chapter 3). As seen from Figure 3, after the burst-events triggered by the surface waves, a silent period follows in the next few days. This might be related to stress drop caused by the burst-events. Afterwards, seismicity quickly returns to background level.

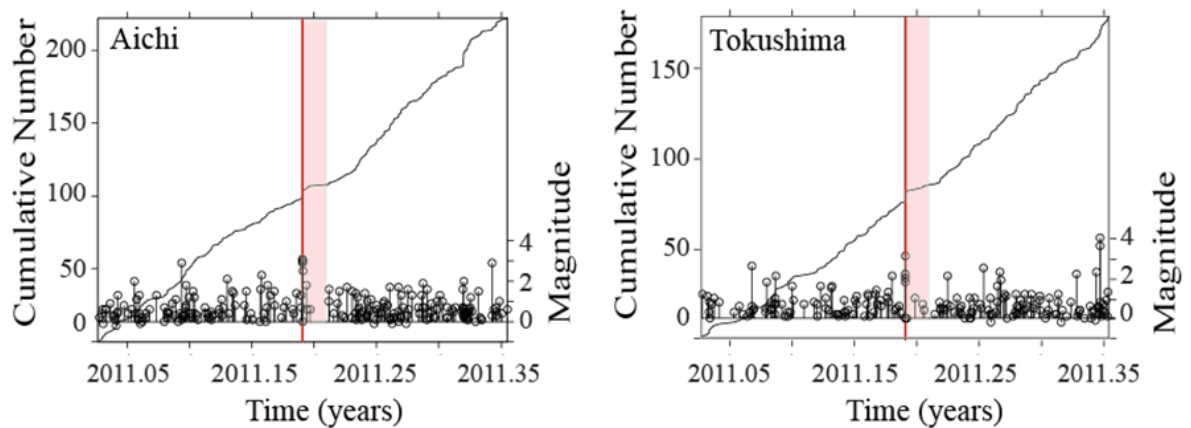


**Figure 3. Seismicity observed at subduction interface areas for 60 days before and after Tohoku-oki earthquake.** The vertical red line represents the occurrence time of Tohoku-oki earthquake, while the red box shows 7 days from the mainshock.

For active faults environment triggering (Figure 4) observed in the other non-volcanic areas, like “Hyogo”, “Tottori” and “Fukuoka”, the seismicity seems to be activated only during the passage of mainshock surface waves (“Hyogo” region), or for a brief interval afterwards.

The immediate seismicity triggering in “Fukuoka” coincides with an area that experienced a large earthquake (M7.0) nearby, in 2005. The short seismic activity in “Tottori” occurred in an area relatively close to a 2016 M6.6 event, where rather frequent moderate-size events often occurred in the past. These observations could support the interpretation that dynamic triggering could be a proxy for detecting areas of relatively high seismic potential (e.g., Enescu et al., 2016).

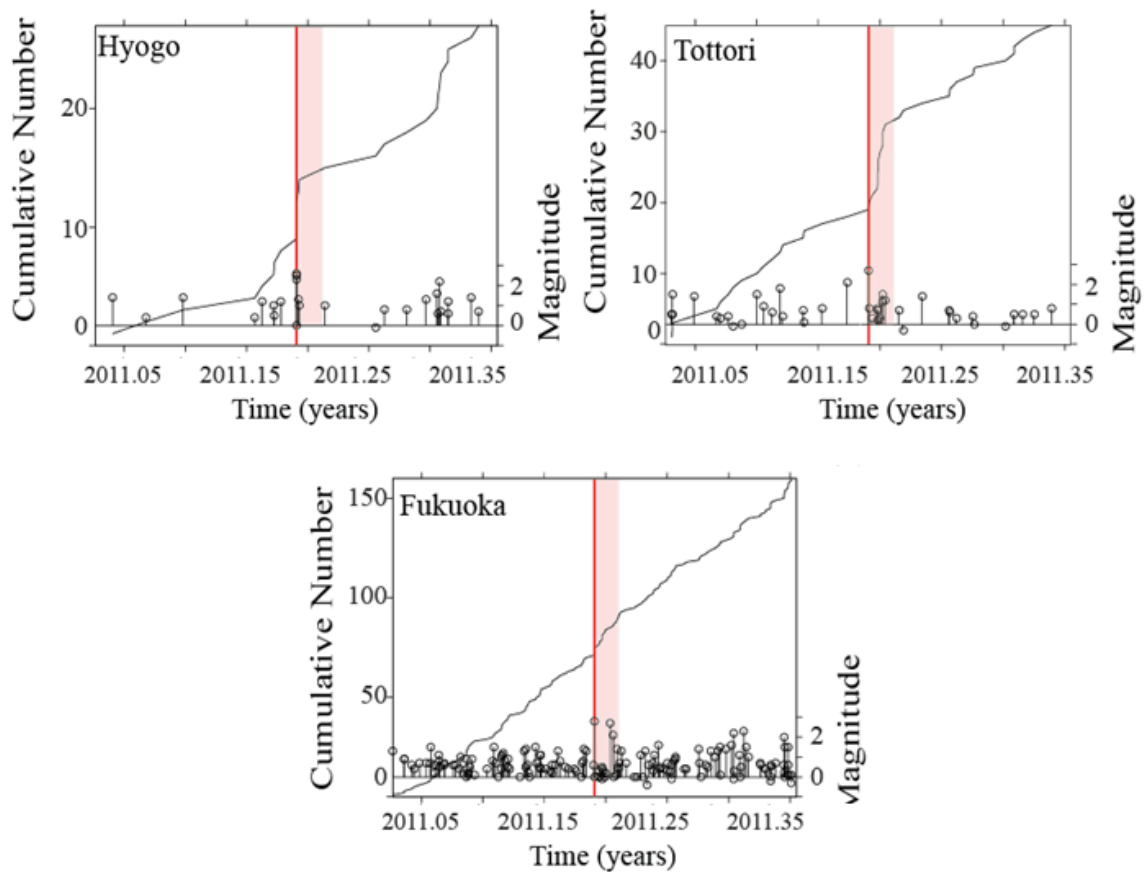


**Figure 4. Seismicity observed at active fault areas for 60 days before and after Tohoku-oki earthquake.** The vertical red line represents the occurrence time of Tohoku-oki earthquake, while the red box shows 7 days from the mainshock.

The regions at or close to volcanoes in Kyushu, labelled as “Oita”, “Nagasaki” and “Kagoshima, were most clearly activated (Figure 5) after the 2011 Tohoku-oki earthquake. Such observations indicate that the higher rates of seismicity after the initial excitation by the surface waves are likely related to local static stress interactions and crustal fluid movement. While the time decay for the stacked earthquake sequence is relatively smooth as seen in the Figure 2, the stair-like pattern observed in the volcanic regions indicate relatively quick and short local activations (possible signature of a fast decay).

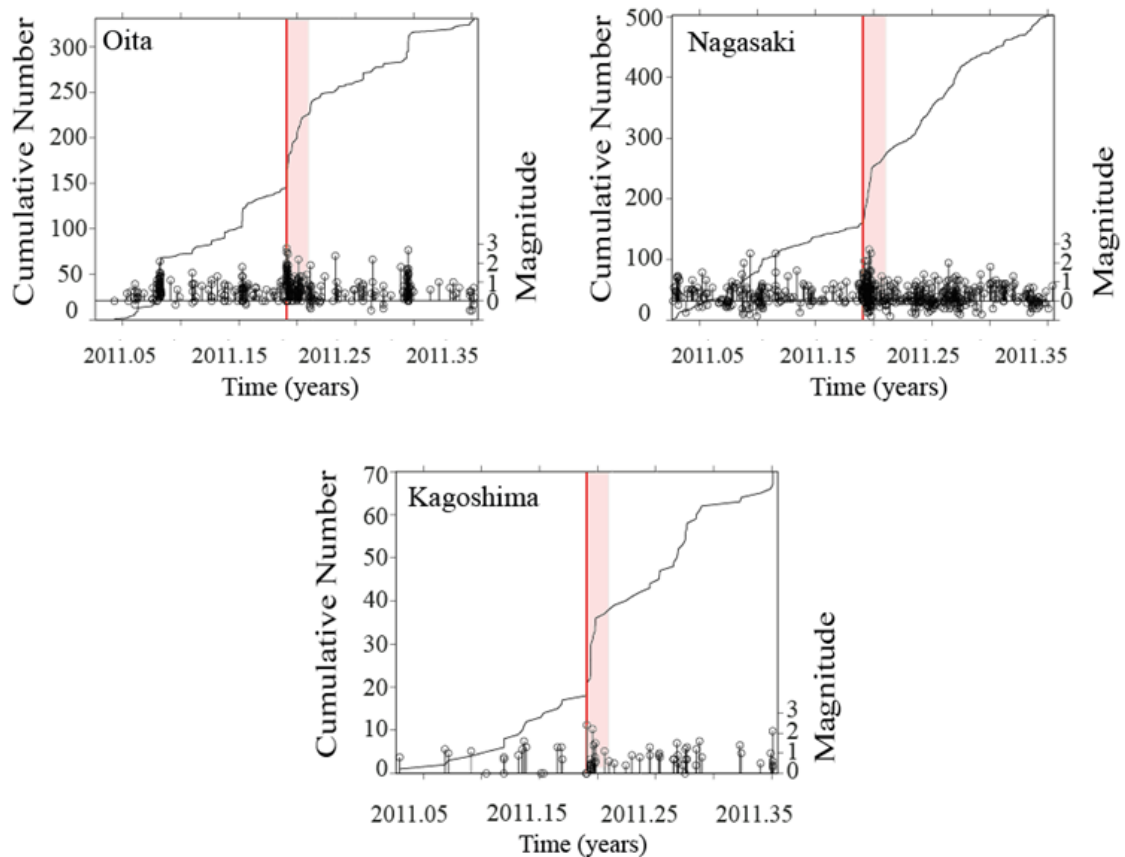


**Figure 5. Seismicity observed in the volcanic regions in Kyushu for 60 days before and after Tohoku-oki earthquake.** The vertical red line represents the occurrence time of Tohoku-oki earthquake, while the red box shows 7 days from the mainshock.

In “Oita” region, the larger events occur at the very beginning of the triggered sequence while in “Nagasaki” region; the first triggered events have smaller magnitudes and are followed by larger events, resembling a seismic swarm sequence.

Following the passage of the surface waves from the megathrust event, local stress interactions (Ziv, 2006) and, excitation of fluids at geothermal and volcanic sites (e.g., Shimojo et al., 2014; Kosuga, 2014) can cause the seismicity rates to remain above the background level however for a relatively brief time. The interpretation is consistent

with other findings) for long-range triggered seismicity that continues after the passage of surface waves (e.g., Brodsky, 2006).

While the immediate post-Tohoku seismicity rate increase is clear in most regions, the Omori-type decay is difficult to identify; this observation contrasts with the results of Figure 2, where stacking enhances the “signal” during the activation period against the background level.

What is the cause of the relatively slow decay of seismicity rates for the stacked sequences? As documented by Aiken and Peng (2014), a relatively slow decay with  $p$ -value  $\sim 0.7$  was observed for the first hour after large teleseismic events which dynamically triggered seismicity at geothermal sites in the United States. Also, slow temporal decay ( $p$ -value  $\sim 0.7$ ) of stacked swarm-like seismic sequences compared with the more typical mainshock-aftershock sequences ( $p$ -values  $\sim 1.0$ ) was reported by Enescu et al., (2009) in California,).

Considering these results, the slow decay observed in this study ( $p$ -value  $\sim 0.7$ ) can be interpreted as the effect of stacking swarm-type seismic sequences triggered predominantly at volcanic or geothermal regions in Kyushu. Some further support for this interpretation comes from the observed trade-off between the  $p$ -value and  $c$ -value of the Modified Omori law.

By fixing the  $p$ -value above 0.7 and inverting only for the  $c$ -value and  $K$ -value, we have observed a tendency of estimated  $c$ -values to increase. For example, a fixed  $p$ -value = 1.0, results in a  $c$ -value = 0.04 days, which is one order larger than the previously determined  $c$ -value (Figure 2). It could be that slightly different timing and decay characteristics of seismicity activation in various areas may result in either a relatively small overall  $p$ -value or large  $c$ -value. Thus, the temporal characteristics of an

individual earthquake cluster might be different than the collective behaviour documented above; however, unfortunately, the number of dynamically activated events is too less for some quantitative local (one-cluster) analysis.

#### **4.5 Fast decay observed at volcanic regions in Kyushu, following the 2016 $M_w$ 7.3 Kumamoto earthquake**

In the previous section, I analysed the stronger activation of seismicity following the 2011 Tohoku-oki earthquake at the region labelled “Oita”. At a closer look, two main sub-areas of activation can be distinguished: one close to Aso volcano and the other one in the north-east, in the Yufuin-Beppu geothermal region.

After the 2016  $M_w$ 7.3 Kumamoto earthquake, the “Oita” area was also seismically activated. Miyazawa (2016), Yoshida (2016) and Uchide et al. (2016) demonstrated the dynamic triggering initiation of seismicity at the Yufuin-Beppu region, where an  $M_w$ 5.9 occurred at very short time after the Kumamoto mainshock; it was followed by many local earthquakes, likely aftershocks of the  $M_w$ 5.9 event.

I show in Figure 6a the aftershocks following the 2016 Kumamoto earthquake, which I divide into three sub-areas. The “Main” area represents where the fault rupture is located, the “Aso” area is close to Aso volcano, at the north-east end of the fault and, the dynamically activated “Yufuin-Beppu” geothermal area, in the north-east.

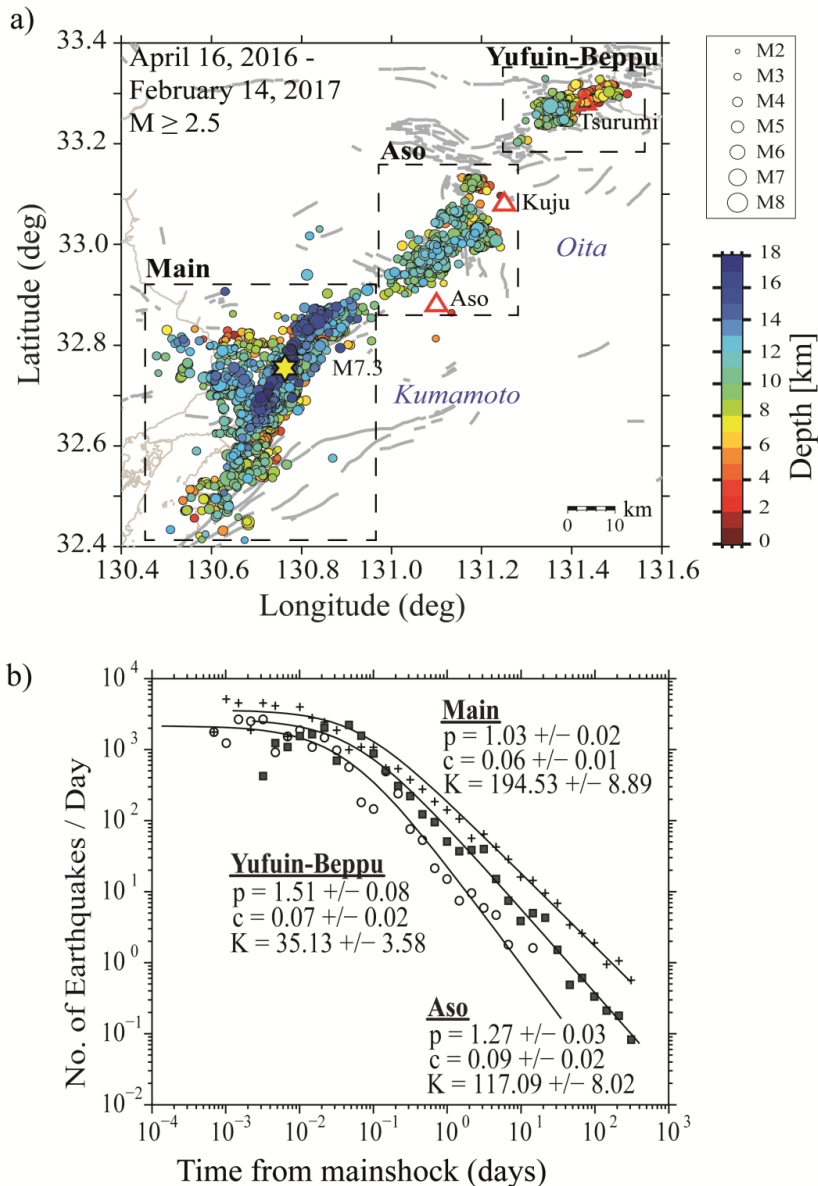


**Figure 6. Spatial distribution and temporal decay for the 2016 Kumamoto aftershock sequence.** a) Distribution of aftershocks of the Mw 7.3 Kumamoto earthquake, from April 16, 2016 to February 14, 2017, coloured as function of depth (with a size scaled with the event magnitude). The three aftershock areas are referred as “Main” for the mainshock (yellow star) region, “Aso” and respectively “Yufuin-Beppu”, for the aftershocks occurred in these two last areas, respectively. Red triangles show volcanos, while grey lines show active faults; b) Aftershock decay and the corresponding Modified Omori Law fit for the three regions indicated in (a).

For these regions, I show in Figure 6b the decay of aftershocks, for selected earthquakes above the completeness magnitude ( $M_c = 2.5$ ). The  $p$ -values at Aso volcano and Yufuin-Beppu geothermal region are relatively high:  $1.27 \pm 0.03$  and  $1.51 \pm 0.08$ , respectively, compared with the aftershock decay in the “Main” area ( $p$ -value of  $1.03 \pm 0.02$ ), which is considered ‘normal value’ for an aftershock sequence.

Considering a threshold magnitude of 3.0, the results are similar, indicating that the results are robust against parameter variations. In a detailed study of Zhuang et al. (2017), regarding the level of magnitude completeness after the 2016 Kumamoto earthquake, he indicates that the  $p$ -values is robust against changes in the threshold magnitude and is not sensitive to completeness issues.

In Figure 7 is shown clearly the short period of activation and fast decay of aftershocks at the Yufuin-Beppu region, when compared with the other two regions. The fast seismicity decay observed around Aso Yufuin-Beppu regions could be interpreted considering the fact that large decay rates ( $p$ -values  $\geq 1.2$ ) of aftershocks are observed near active volcanic centres, where are associated with faster stress relaxation following mainshocks and higher temperatures near shallow magma reservoirs (Klein et al., 2006).

Moreover, the occurrence of the relatively large aftershock ( $M_w 5.9$ ) at the “Yufuin-Beppu” region could have released completely the accumulated tectonic stresses (i.e., almost complete stress drop), explaining the quick attenuation and weak seismic activity after one month from the mainshock occurrence time (see Figure 7).

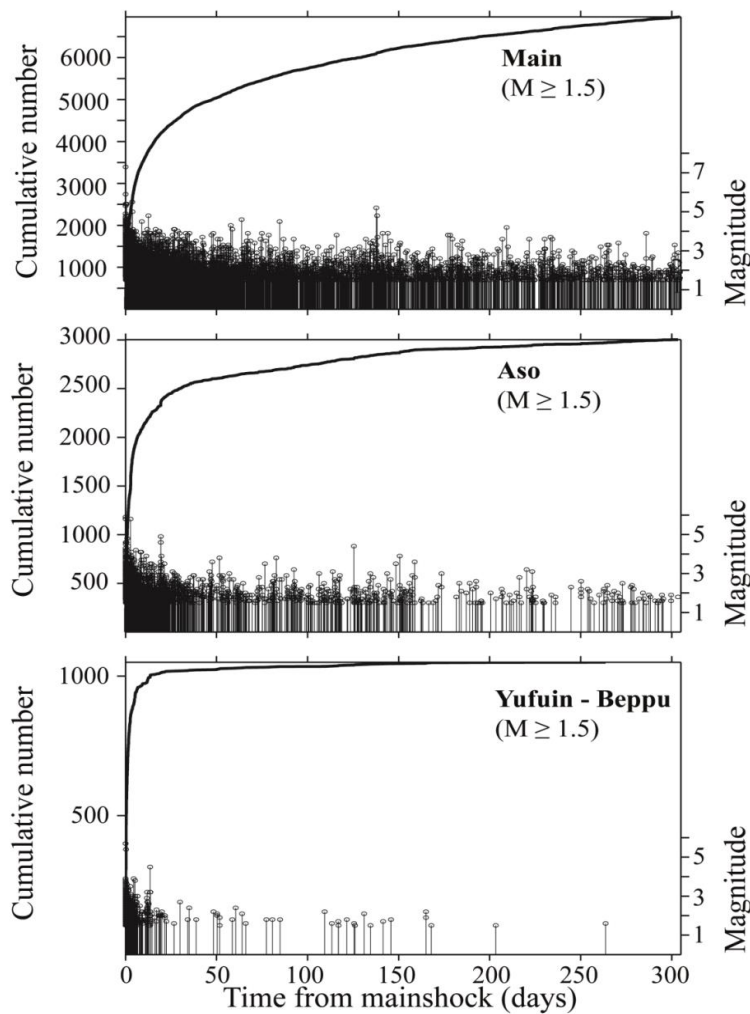


**Figure 7. Aftershock spatial distribution and temporal decay for the 2016 Kumamoto sequence.** Magnitude versus time plot for the “Main”, “Aso” and “Yufuin-Beppu” regions ( $M \geq 1.5$ ).

Finally, in an attempt to integrate the observations on the decay of dynamically activated seismicity at geothermal and volcanic areas in Kyushu, following the 2011  $M_w$  Tohoku-oki earthquake, I suggest that the overall temporal decay of seismicity rates follows the Modified Omori Law and the estimated small  $p$ -value are an effect of stacking sequences with different temporal characteristics (including different seismicity rate decays).

The vigorous seismicity after the Kumamoto earthquake displayed clear contrasting aftershock decays: large  $p$ -values at volcanic/geo-thermal regions and ‘normal’  $p$ -values around the mainshock rupture. A fast decay was observed in the Yufuin-Beppu region, following a dynamically triggered relatively large aftershock.

While large surface waves from mainshock could dynamically trigger the  $M_w$  5.9 event (e.g., Miyazawa, 2016), the fast decay and the abrupt termination of aftershocks was probably caused by local conditions, such as stress release and increased temperature, as seen from the local heat-flow map shown in Figure 8.

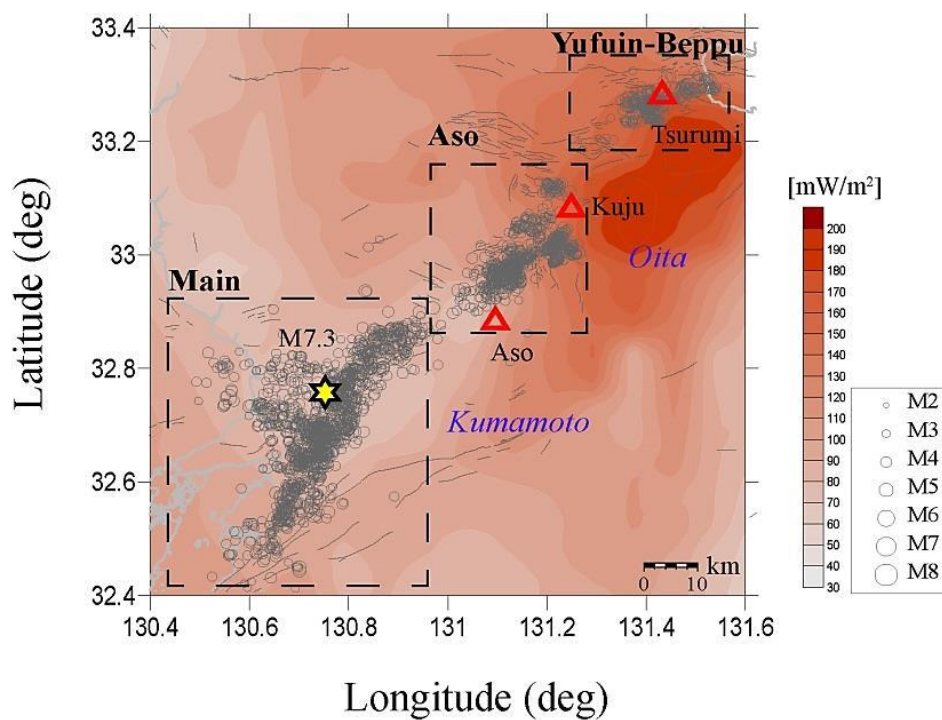


**Figure 8. Heat flow map around Aso and Yufuin-Beppu volcanic regions.** Earthquake (grey circles) and volcano (red triangle) distribution following the 2016 Kumamoto earthquake (yellow star) overlaid on top of interpolated map of JMA heat-flow data (Matsumoto, 2007)

## 4.6 Conclusions

By creating and analysing the a combined catalogue of events for the remote seismicity observed after the 2011  $M_w$  9.0 Tohoku-oki earthquake and the events recorded by JMA, I show that the stacked seismicity had a clear, but weak increase immediately after the megathrust earthquake, which continued after the passage of seismic waves, for a period of about 7 days or less, depending on the tectonic environment where the triggering occurred.. The decay of activated-earthquake rates towards the pre-mainshock levels follows the Modified Omori law and is relatively slow, with  $p$ -values of about 0.7, possibly indicating the stacking of swarm-like triggered sequences.

In areas close to the subduction interface, (Aichi and Tokushima), I observed burst-events followed by a silent period, probably caused by stress-drop, while the active fault environment areas (Hyogo, Tottori, Fukuoka), were characterized by an instant activation due to the shearing motion of the surface waves.

The most evident seismicity rate increase was observed in in three volcanic/geothermal regions in Kyushu: Nagasaki, Oita (includes Aso volcano area and the Yufuin-Beppu geothermal area), and Kagoshima (at the Ibusuki volcanic field).

Finally, following the M7.3 Kumamoto earthquake, the aftershock analysis around Aso volcano Yufuin-Beppu region, revealed a fast decay of aftershock rates ( $p$ -value  $\geq 1.2$ ), which can be interpreted as rapid stress relaxation near high-temperature, shallow magmatic reservoirs. Future studies should help in assessing whether the fast decay is a common feature for dynamically triggered events at geothermal/volcanic sites

## Chapter 5

### Discussion and Conclusions

I identified several places where the seismic waves from the 2011 M9.0 Tohoku-Oki earthquake triggered seismicity during and after the passing of the waves. The observations on the distribution of remote seismic activation in SW Japan, clearly demonstrate a similar behaviour in time for sequences which occur in similar tectonic environments.

The first events in each of the triggered areas in Southwest Japan occur during the passage of large Love and Rayleigh waves from the mainshock. I have observed that the amplitudes of surface wave displacements on transverse components are significantly larger than those on vertical or radial components and hypothesized that the Love waves played a significant role in initiating remotely the seismicity activation after the megathrust event. The shearing-motion due to larger amplitudes of Love waves on well-lubricated local faults may have facilitated and started failure; the subsequent passage of Rayleigh waves triggered also local earthquakes.

I also estimate the peak dynamic stress changes associated with the passage of Rayleigh and Love waves in the triggered regions from the amplitudes of the surface wave ground velocities (e.g., Peng et al. 2009). After the occurrence of the 2011 Tohoku-oki earthquake, the values calculated for the transverse component, corresponding to Love waves (Figure 1, Chapter 3 ) are significantly larger than those calculated for vertical components, implying that the triggering potential of Love wave is higher.

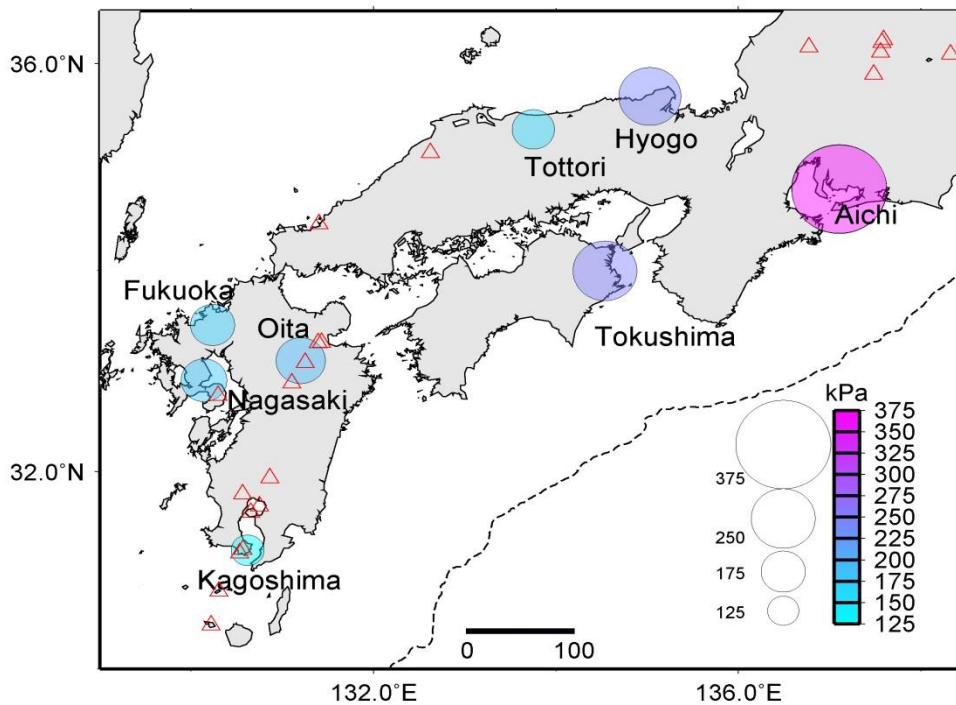


**Figure 1. Maximum dynamic stress changes in SW Japan due to the passage of surface waves from the 2011 Tohoku-oki earthquake.**

Enescu et al.(2016) documented relatively widespread remote triggering of seismicity also following the 2016 Kumamoto earthquake, during the passage of the surface waves from the mainshock. The dynamic stresses in the triggered regions range from several kPa to tens of kPa, values that are smaller than those observed for the 2011 Tohoku-oki earthquake. Since most of the remotely triggered earthquakes were observed at volcanoes, we suggest that the excitation of fluids may have been the main triggering mechanism in these regions.

In volcanic and geothermal areas, recovery times may be further shortened by episodic advection of thermal fluids into the crust from the lower crust or upper mantle that serve as local stress sources.

Shorter recovery times mean that, at any given time, more areas are likely to be hovering in a near-critical state and thus susceptible to triggering by small dynamic stresses than in areas with low strain rates and extended recovery times.

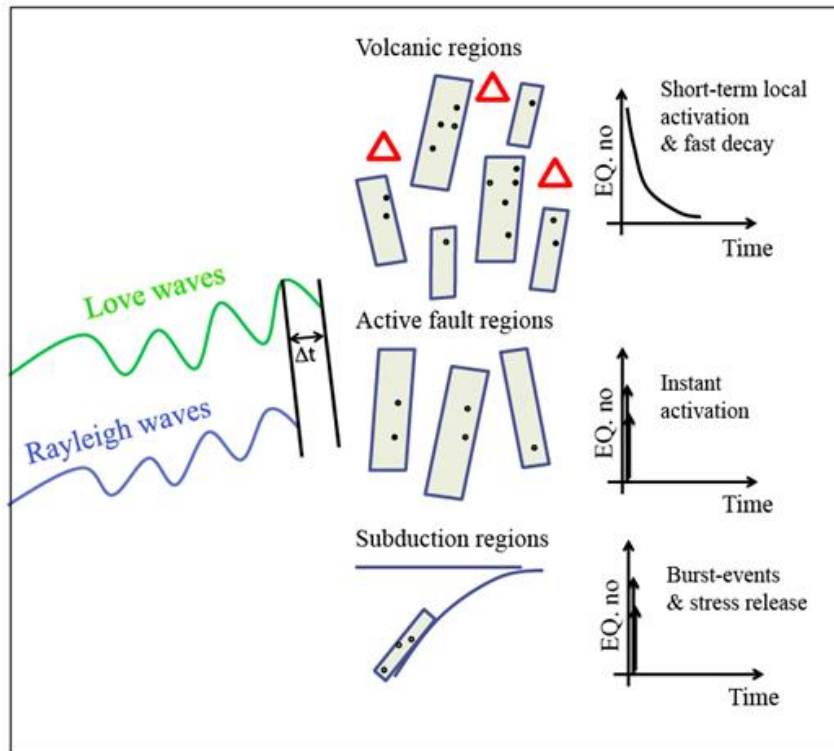


**Figure 2. Triggering model for observed seismicity in SW Japan, for different tectonic environments**

- Triggering is initiated on local fractures by shearing motion at the arrival of Love waves. Triggering continues during the passage of Rayleigh waves;
- In volcanic regions (Nagasaki, Oita, Kagoshima), local triggering due to static stress changes/fluid excitation continues for the following few days.
- In active fault regions (Hyogo, Tottori, Fukuoka), instant activation by frictional failure is observed.
- In subduction regions (Aichi, Tokushima), burst-events cause a stress-drop that is followed by a silent period for the next few days.

Next, I tried to integrate the results in a possible triggering scenario (Figure 2) that would include all the observations on remote triggering in Southwest Japan due to the passage of surface waves from the 2011 Tohoku-oki earthquake.

As for aftershock decay characteristics, many observational and theoretical studies have linked p-value or changes in p-value to variations of material parameters, variations in the state of stress, and changes in the seismic cycle. For example, aftershock generation models predict  $0.8 < p < 1.5$  depending on uniformity of stress changes, heterogeneity of fault strength, and relaxation of stresses (Dietrich, 1994).

Unfortunately, the number of dynamically activated events in each remotely triggered region is too less for each individual cluster analysis. As in Davis and Frohlich (1991), a stacked sequence is the superposition of many isolated aftershock sequences. Stacking aftershock sequences allows us to determine p-values for sequences possessing too few events to allow meaningful analysis on an individual basis, but the meaning of this p-value is not well understood so far.

Only a few investigations have focused on stacked sequences. These include Gross and Kisslinger (1994), who stack synthetic sequences generated according to a stretched exponential decay relation, and Davis and Frohlich (1991), who stack all sequences in a region to determine an averaged p-value. However, so far, there is no study examining stacking remotely triggered seismic activity.

The stacked seismicity had a clear, but weak increase immediately after the Tohoku-oki earthquake, that continued for a period of about one week or less, following the Modified Omori law (with relatively slow decay, possibly due to stacking of all triggered sequences).

The results suggest that despite an overall slow decay of seismicity rates, the weak seismicity activation in the studied areas returns to the background level after a relatively short period. Nevertheless, the temporal characteristics of an individual earthquake cluster might be different than the collective behaviour documented above, especially in volcanic and geothermal regions.

Since one of the most activated areas was in Oita region, I analysed the aftershock decay in the same region after the occurrence of the 2016 M7.3 Kumamoto earthquake. Around Aso volcano and at the Yufuin-Beppu geothermal region, the fast decay rate of aftershock rates suggests quick stress relaxation nearby high-temperature, shallow magmatic reservoirs.

The same rapid aftershocks decay was also observed in the other studied area, in Shizuoka region, around Mount Fuji. Although the triggering mechanism for this earthquake generation was completely different and challenging to identify, the fast aftershock decay indicates fast stress relaxation associated with heat-flow values.

Dynamic triggering studies may help to estimate seismic hazards by further understanding the earthquake cycle through tectonic tremor and by identifying near-critical conditions on faults through remotely triggered earthquakes. The interplay of Rayleigh waves and crustal fluids requires more research, especially to better understand earthquake-volcano interactions.

A better understanding of remote triggering will help to describe the short-term processes that lead to slip nucleation and generation of earthquakes and thereby can potentially lead towards better techniques for earthquake prediction. Subduction zones repeatedly generate strong earthquakes which influence the neighbouring volcanic arc.

Research focusing on earthquake-volcano interaction will result in better knowledge of the conditions leading to triggered volcanic unrest.

## **Acknowledgements**

For the last 3 and half years, I received total and unconditional support from my academic advisor, Professor Bogdan Dumitru Enescu. He has been from the very beginning a mentor, helping me not only with my research pursuit, but also with the challenges that arise from living in a foreign country. He encouraged me to overcome all the difficulties, and even offered me the chance to be a part of two great academic environments at two universities in Japan, University of Tsukuba and Kyoto University. His support was not just academically, but also professionally, always encouraging me to explore all professional opportunities. I am extremely grateful to him and I could never express my true appreciation.

I am very thankful to my other supervisor, Professor Yuji Yagi, who gave me his guidance and encouragements throughout my time spend in his laboratory at University of Tsukuba. All the colleagues from this laboratory were very supportive, and I would like to express a special thank you to Ryo Okuwaki who helped me countless times, even before I arrived in Japan. I am grateful to Professor Kenchiro Hisada for always being so helpful and agreeing to serve on my thesis committee.

I would also like to express my gratitude to all the professors and academic division members from the two universities, who offered me their constant support. I am grateful to the Japanese Ministry of Education, Culture, Sports, Science, and Technology (MEXT) for providing a “Monbukagakusho” scholarship for studying at the University of Tsukuba, Japan.

Not lastly, I am grateful for being allowed to use JMA catalogue and NIED waveform data in my study. With the help of my supervisor Bogdan Enescu, I was able to get support from these two institutions whenever required. I thank Sachiko Tanaka, Katsuhiko Shiomi (NIED), and all the other researchers that offered me precious data and insight into Japanese seismology.

## References

- Aiken C., Peng Z., 2014. Dynamic triggering of microearthquakes in three geothermal regions of California, *J. Geophys. Res.*, 119, 6992–7009, doi:[10.1002/2014JB011218](https://doi.org/10.1002/2014JB011218).
- Aizawa K., Sumino H., Uyeshima M., Yamaya Y., Hase H., Takahashi H. A., Ogawa Y., 2016. Gas pathways and remotely triggered earthquakes beneath Mount Fuji, Japan. *Geology*, 44(2), 127-130. doi: [10.1130/G37313.1](https://doi.org/10.1130/G37313.1)
- Aki K., 1965. Maximum likelihood estimate of b in the formula  $\log N = a - bM$  and its confidence level, *Bull. Earthq. Res. Inst.*, 43, 237–239.
- Aki K, Richards P., 2002. Quantitative seismology, 2nd edn. *University Science Books*, Freeman, San Francisco
- Brodsky E. E., 2006. Long-range triggered earthquakes that continue after the wave train passes, *Geophys. Res. Lett.*, 33, L15313, doi:[10.1029/2006GL026605](https://doi.org/10.1029/2006GL026605).
- Brodsky E.E., Karakostas V., and Kanamori H., 2000. A new observation of dynamically triggered regional seismicity: Earthquakes in Greece following the August 1999 Izmit, Turkey earthquake, *Geophys. Res. Lett.*, 27, 2741–2744, doi:[10.1029/2000GL011534](https://doi.org/10.1029/2000GL011534).
- Brodsky E. E., and Prejean S. G., 2005. New constraints on mechanisms of remotely triggered seismicity at Long Valley Caldera, *J. Geophys. Res.*, 110, B04302, doi:[10.1029/2004JB003211](https://doi.org/10.1029/2004JB003211).

Chao K., and Obara, K., 2016. Triggered tectonic tremor in various types of fault systems of Japan following the 2012 Mw8.6 Sumatra earthquake, *J. Geophys. Res.*, 121, 170 – 187, doi:10.1002/2015JB012566.

Chao K., Peng Z., Gonzalez-Huizar H., Aiken C., Enescu B., Kao H., Velasco A. A., Obara K., Matsuzawa T., 2013. A global search for triggered tremor following the 2011 Mw 9.0 Tohoku earthquake, *Bull. Seismol. Soc. Am.*, 103, 1551–1571, doi:10.1785/0120120171.

Dieterich J.H. , 1994. A constitutive law for rate of earthquake production and its application to earthquake clustering, *J. Geophys. Res.* , 99 , 2601-2618.

Enescu B., Mori J., and Miyazawa M., 2007. Quantifying early aftershock activity of the 2004 mid-Niigata Prefecture earthquake (Mw6.6), *J. Geophys. Res.*, doi:10.1029/2006JB004629

Enescu B., Hainzl S., Ben-Zion Y., 2009. Correlations of seismicity patterns in Southern California with surface heat flow data, *Bull. Seismol. Soc. Am.*, 99(6), 3114-3123, doi:10.1785/0120080038.

Enescu B., Aoi S., Toda S., Suzuki W., Obara K., Shiomi K., Takeda T., 2012. Stress perturbations and seismic response associated with the 2011 M9.0 Tohoku-oki earthquake in and around the Tokai seismic gap, central Japan, *Geophys. Res. Lett.*, 39, L00G28, doi:10.1029/2012GL051839.

Enescu B., Shimojo K., Opris A., Yagi Y., 2016. Remote triggering of seismicity at Japanese volcanoes following the 2016 M7.3 Kumamoto earthquake, *Earth Planets Space*, 68:165, doi:10.1186/s40623-016-0539-5.

Fujii, T., 2007. Magmatology of Fuji Volcano [in Japanese with English abstract], in *Fuji Volcano*, pp. 233–244, Yamanashi Institute of Environmental Sciences, Fuji-Yoshida, Japan.

Fujita E. K., Ueda T., Kohno H., Yoshioka Y., Toda S., Kikuchi N., Ida Y., 2013. Stress field change around the Mount Fuji volcano magma system caused by the Tohoku megathrust earthquake, *Japan: Bulletin of Volcanology*, v. 75, p. 679–693, doi:[10.1007/s00445-012-0679-9](https://doi.org/10.1007/s00445-012-0679-9).

Gonzalez-Huizar H., Velasco A. A., 2011. Dynamic triggering: Stress modeling and a case study, *J. Geophys. Res.*, 116, B02304, doi:[10.1029/2009JB007000](https://doi.org/10.1029/2009JB007000).

Harrington R.M., Brodsky E.E., 2006. The absence of remotely triggered seismicity in Japan, *Bull. Seismol. Soc. Am.*, 96(3), 871–878, doi:[10.1785/0120050076](https://doi.org/10.1785/0120050076).

Harris R. A., 1998. Introduction to a special section: Stress triggers, stress shadows, and implications for seismic hazards, *J. Geophys. Res.* 103, 24,347–24,358

Hill D.P., Reasenber P.A., Michael A., Arabaz W.J., Beroza G., Brumbaugh D., Brune J.N., Castro R., Davis S., dePolo D., Ellsworth W.L., Gomberg J., Harmsen S., House L., Jackson S.M., Johnston M.J.S., Jones L., Keller R., Malone S., Munguia L., Nava S., Pechmann J.C., Sanford A., Simpson R.W., Smith R.B., Stark M., Stickney M., Vidal A., Walter S., Wong V., Zollweg J., 1993. Seismicity remotely triggered by the magnitude 7.3 Landers, California, Earthquake, *Science*, 260, 1617–1623, doi:[10.1126/science.260.5114.1617](https://doi.org/10.1126/science.260.5114.1617).

Hill D., Prejean S., 2015. Dynamic triggering, *Treatise on Geophysics*, 2nd ed., edited by G. Schubert, Elsevier, Amsterdam, vol. 4, 273–304, doi:10.1016/B978-0-444-53802-4.00078-6.

Hirata N., Matsu'ura, M., 1987. Maximum-likelihood estimation of hypocenter with origin time eliminated using nonlinear inversion technique, *Phys. Earth Planet. Inter.*, **47**, 50–61.

Hirose F., Nakajima J., Hasegawa A., 2008. Three-dimensional seismic velocity structure and configuration of the Philippine Sea slab in southwestern Japan estimated by double-difference tomography, *J. Geophys. Res.*, 113, B09315, doi:10.1029/2007JB005274.

Jaeger J.C., Cook N.G.W., 1979. Fundamentals of rock mechanics, 3rd edition. Chapman\_& Hall.

Kagan Y. Y., 2004. Short-term properties of earthquake catalogues and models of earthquake source, *Bull. Seismol. Soc. Am.*, 94, 1207 –1228.

Kaneko T., Yasuda A., Fujii T., and Yoshimoto M., 2010. Crypto-magma chambers beneath Mt. Fuji, *J. Volcanol. Geotherm. Res.*, 193, 161–170, doi:10.1016/j.jvolgeores.2010.04.002.

Kato A., Fukuda J.I., and Obara K., 2013. Response of seismicity to static and dynamic stress changes induced by the 2011 M9.0 Tohoku-Oki earthquake, *Geophys. Res. Lett.*, 40, 3572–3578, doi:10.1002/grl.50699.

Kisslinger C. and Jones M. L., 1991. Properties of aftershocks in southern California, *J. Geophys. Res.*, 96, 11947–11958.

- Klein F.W., Wright T. L., Nakata J., 2006. Aftershock decay, productivity and stress rates in Hawaii: Indicators of temperature and stress from magma sources, *J. Geophys. Res.*, 111, B07307, doi:[10.1029/2005JB003949](https://doi.org/10.1029/2005JB003949).
- Kosuga M., 2014. Seismic activity near the Moriyoshi-zan volcano in Akita Prefecture, northeastern Japan: implications for geofluid migration and a midcrustal geofluid reservoir, *Earth Planets Space*, 66:77, doi:[10.1186/1880-5981-66-77](https://doi.org/10.1186/1880-5981-66-77).
- King G., Stein R., and Lin J., 1994. Static stress changes and the triggering of earthquakes, *Bull. Seismol. Soc. Am.*, 84(3), 935–953.
- Kumazawa T., and Ogata Y., 2013. Quantitative description of induced seismic activity before and after the 2011 Tohoku-Oki earthquake by nonstationary ETAS models, *J. Geophys. Res. Solid Earth*, 118, 6165–6182, doi:[10.1002/2013JB010259](https://doi.org/10.1002/2013JB010259).
- Maeda T., Obara K., Furumura T., Saito T., 2011. Interference of long-period seismic wavefield observed by the dense Hi-net array in Japan, *J Geophys Res.*, 116, B10303, doi:[10.1029/2011JB008464](https://doi.org/10.1029/2011JB008464).
- Manga M., and Brodsky E. E., 2006. Seismic triggering of eruptions in the far field: Volcanoes and geysers, *Annu. Rev. Earth Planet. Sci.*, 34, 263 – 291.
- Marzocchi W., Casarotti E., and Piersanti A. , 2002. Modelling the stress variations induced by great earthquakes on the largest volcanic eruptions of the 20th century, *J. Geophys. Res.*, 107 (11), 2320, doi:[10.1029/2001JB001391](https://doi.org/10.1029/2001JB001391).
- Matsumoto T., 2007. Terrestrial heat flow distribution in Japan area based on the temperature logging in the borehole of NIED Hi-net, *American Geophysical Union*, Fall Meeting 2007, abstract #T23A-1217.

Mikumo T. and Miyatake T., 1979. Earthquake sequences on a frictional fault model with non-uniform strengths and relaxation times, *Geophys. J. R. Astron. Soc.*, 59, 497–522.

Miyazawa M., 2011. Propagation of an earthquake triggering front from the 2011 Tohoku-Oki earthquake, *Geophys. Res. Lett.*, 38:L23307, doi:10.1029/2011GL049795.

Miyazawa M., 2016. An investigation into the remote triggering of the Oita earthquake by the 2016 Mw 7.0 Kumamoto earthquake using full wavefield simulation, *Earth Planets Space*, 68:205, doi:10.1186/s40623-016-0585-z.

Mogi K., 1962. Study of the elastic shocks caused by the fracture of heterogeneous materials and its relation to earthquake phenomena, *Bull. Earthq. Res. Inst., Univ. Tokyo*, 40, 125–173.

Mogi, K., 1967. Earthquakes and fractures, *Tectonophys.*, 5, 35–55.

Nanjo K., Nagahama H., and Satomura M., 1998. Rates of aftershock decay and the fractal structure of active fault systems, *Tectonophysics*, 287, 173 – 186

Nakamichi H., Watanabe H., Ohminato T., 2007. Three-dimensional velocity structures of Mount Fuji and the South Fossa Magna, central Japan: *Journal of Geophysical Research* , v. 112, B03310, doi:10.1029/2005JB004161.

Nostro C, Stein RS, Cocco M, Belardinelli ME, Marzocchi W. 1998. Two-way coupling between Vesuvius eruptions and southern Apennine earthquakes, Italy, by elastic stress transfer, *J. Geophys. Res.* 103:24487–504

Nyffenegger P., and Frohlich C., 1998. Recommendations for Determining p Values for Aftershock Sequences and Catalogs, *Bull. Seismol. Soc. Am.*, 88, 1144-1154.

Omori F., 1894. On the aftershocks of earthquakes, *Journal of the College of Science, Imperial University of Tokyo*, vol. 7, 111–200.

Ogata Y., 1983. Estimation of the parameters in the modified Omori formula for aftershock frequencies by maximum likelihood procedure, *J. Phys. Earth*, 31, 115-124.

Peng Z., Vidale J. E., and Houston H., 2006. Anomalous early aftershock decay rate of the 2004 Mw6.0 Parkfield, California, earthquake, *Geophys. Res. Lett.*, 33, L17307, doi:[10.1029/2006GL026744](https://doi.org/10.1029/2006GL026744).

Peng Z., and Zhao P., 2009. Migration of early aftershocks following the 2004 Parkfield earthquake, *Nature Geoscience.*, 2, 877-881, doi:[10.1038/ngeo697](https://doi.org/10.1038/ngeo697).

Peng Z., Vidale J.E., Wech A. G., Nadeau R. M., Creager K. C., 2009. Remote triggering of tremor along the San Andreas Fault in central California, *J. Geophys. Res.*, 114, B00A06, doi:[10.1029/2008JB006049](https://doi.org/10.1029/2008JB006049).

Shelly D. R., Beroza G. C., and Ide S., 2007. Non-volcanic tremor and low-frequency earthquake swarms. *Nature* 446, 305–307, doi:[10.1038/nature05666](https://doi.org/10.1038/nature05666).

Shimojo K., Enescu B., Yagi Y., Takeda T., 2014. Fluid-driven seismicity activation in northern Nagano region after the 2011 M9.0 Tohoku-oki earthquake, *Geophys. Res. Lett.*, 41, 7524–7531, doi:[10.1002/2014GL061763](https://doi.org/10.1002/2014GL061763).

Stein R. S., 1999. The role of stress transfer in earthquake occurrence, *Nature*, 402, 605–609.

- Suzuki W., Aoi S., Sekiguchi H., Kunugi T., 2011. Rupture process of the 2011 Tohoku-Oki mega-thrust earthquake (M9.0) inverted from strong-motion data, *Geophys. Res. Lett.*, 38, L00G16, doi:10.1029/2011GL049136.
- Terakawa T., and Matsu'ura M., 2010. The 3-D tectonic stress fields in and around Japan inverted from centroid moment tensor data of seismic events, *Tectonics*, 29, TC6008, doi:10.1029/2009TC002626.
- Toda S., Stein R. S., Lin J., 2011. Widespread seismicity excitation throughout central Japan following the 2011 M=9.0 Tohoku earthquake and its interpretation by Coulomb stress transfer, *Geophys. Res. Lett.*, 38, L00G03, doi:10.1029/2011GL047834.
- Toda S., and Enescu B., 2011. Rate/state Coulomb stress transfer model for the CSEP Japan seismicity forecast, *Earth Planet Space*, 63:2, doi:10.5047/eps.2011.01.004.
- Uchide T., Horikawa H., Nakai M., Matsushita R., Shigematsu N., Ando R., Imanishi K., 2016. The 2016 Kumamoto–Oita earthquake sequence: aftershock seismicity gap and dynamic triggering in volcanic areas, *Earth Planets Space*, 68:180, doi:10.1186/s40623-016-0556-4
- Ukawa M., 2005. Deep low-frequency earthquake swarm in the mid crust beneath Mount Fuji (Japan) in 2000 and 2001. *Bull Volcano*, 168:47–56
- Utsu T., 1961. A statistical study on the occurrence of aftershocks, *Geophys. Mag.* 30, 521~05.
- Utsu T., Ogata Y., Matsu'ura R. S., 1995. The Centenary of the Omori Formula for a Decay Law of Aftershock Activity, *J. Phys. Earth* 43, 1-33.

- Woessner, J., Wiemer S., 2005. Assessing the quality of earthquake catalogues: Estimating the magnitude of completeness and its uncertainty, *Bull. Seismol. Soc. Am.*, 95, doi:[10.1785/0120400007](https://doi.org/10.1785/0120400007).
- Yagi Y., and Fukahata Y., 2011. Rupture process of the 2011 Tohoku-oki earthquake and absolute elastic strain release, *Geophys. Res. Lett.*, 38, L19307, doi:[10.1029/2011GL048701](https://doi.org/10.1029/2011GL048701).
- Yagi Y., Okuwaki R., Enescu B., Kasahara A., Miyakawa A., Otsubo M., 2016. Rupture process of the 2016 Kumamoto earthquake in relation to the thermal structure around Aso volcano, *Earth Planets Space*, 68:118, doi:[10.1186/s40623-016-0492-3](https://doi.org/10.1186/s40623-016-0492-3)
- Yamashita T., and Knopoff L., 1987. Models of aftershock occurrence, *Geophys. J. R. Astron. Soc.*, 91, 13 – 26.
- Yamashita T., 2003. Regularity and complexity of aftershock occurrence due to mechanical interactions between fault slip and fluid flow. *Geophys J Int* 152:20–33.
- Yoshida S., 2016. Earthquakes in Oita triggered by the 2016 M7.3 Kumamoto earthquake, *Earth Planets and Space*, 68:176, doi:[10.1186/s40623-016-0552-8](https://doi.org/10.1186/s40623-016-0552-8)
- Yoshimoto, M., Fujii, T., Kaneko, T., Yasuda, A., Nakada, S. and Matsumoto, A., 2010. Evolution of Mount Fuji, Japan: Inference from drilling into the subaerial oldest volcano, pre-Komitake. *Island Arc*, vol.19, p.470-488
- Yukutake Y., Honda R., Harada M., Aketagawa T., Ito H., Yoshida A., 2011. Remotely-triggered seismicity in the Hakone volcano following the 2011 off the Pacific coast of Tohoku earthquake, *Earth Planets Space*, 63, 737–740, doi:[10.5047/eps.2011.05.004](https://doi.org/10.5047/eps.2011.05.004).

Yukutake Y., Miyazawa M., Honda R., Harada M., Ito H., Sakaue M., Koketsu K., Yoshida A., 2013. Remotely triggered seismic activity in Hakone volcano during and after the passage of surface waves from the 2011 M9.0 Tohoku-Oki earthquake, *Earth Planet Sc. Lett.*, 373, 205–216, doi:[10.1016/j.epsl.2013.05.004](https://doi.org/10.1016/j.epsl.2013.05.004).

Ziv A., 2006. On the Role of Multiple Interactions in Remote Aftershock Triggering: The Landers and the Hector Mine Case Studies, *Bull. Seismol. Soc. Am.*, 96(1), 80–89, doi:[10.1785/0120050029](https://doi.org/10.1785/0120050029).

Zhuang, J., Ogata, Y., Wang, T., 2017. Data completeness of the Kumamoto earthquake sequence in the JMA catalog and its influence on the estimation of the ETAS parameters. *Earth, Planets and Space*, 69:36, doi:[10.1186/s40623-017-0614-6](https://doi.org/10.1186/s40623-017-0614-6).